energy&fuels

pubs.acs.org/EF Review

Recent Advances in Titanium Niobium Oxide Anodes for High-Power Lithium-Ion Batteries

Tao Yuan, Luke Soule, Bote Zhao, Jie Zou, Junhe Yang, Meilin Liu,* and Shiyou Zheng*

Cite This: *Energy Fuels* 2020, 34, 13321−13334 Read Online

ABSTRACT: High-power energy storage devices are required for many emerging technologies. The rate capability of existing energy storage devices is inadequate to fulfill the requirements of fast charging and discharging while maintaining suitable long-term stability and energy density. This is readily apparent when evaluating the current anode of choice, graphite, which does not have an acceptable high-rate capability using traditional electrolytes. Recent work has shown that titanium niobium oxides (TNO) are promising alternative anode materials with high charge/discharge rates, excellent stability, and reasonable capacity. This article reviews the latest advancements in the development of TNO-based anode materials and architectures for fast energy storage devices, including new insights into understanding their crystal structure and lithiation mechanisms, effective strategies to improve the electrochemical properties of the materials (e.g., defect engineering, composite design, and overlithiation), and rational design of electrode and cell architectures to facilitate fast charge and mass transfer. Critical challenges and new directions in achieving high rate capabilities will also be discussed.

1. INTRODUCTION

Given the urgency of issues such as global warming, diminishing supplies of fossil fuels, and the prevalence of air pollution, the demand for carbon-free energy and transportation has been growing rapidly.[1] Current carbon-free, renewable energy technologies such as wind and solar power suffer from issues related to their intermittent nature.[2] It has been proposed that electrochemical energy storage systems can help mitigate this issue through technologies such as stationary smart grids. In addition, electrochemical energy storage systems are key to the development of mobile electric vehicles (EV), which are an important technology for promoting carbon-free transportation.[3]

Lithium-ion batteries (LIBs) have achieved success due to their high energy and power density and long cycle life. The most common commercial materials used as cathodes and anodes for LIBs are $LiCoO_2$ and carbon-based materials (typically graphite), respectively.[4] $LiCoO_2$ cathodes are currently being replaced by $LiNi_{1/3}Co_{1/3}Mn_{1/3}O_2$, $LiFePO_4$, and $LiMn_2O_4$ in order to maximize energy and/or power density and minimize cost and safety concerns.[5−7] A recent study has found that the anode, graphite, is the rate-limiting material for fast-charging LIBs for EVs.[8] Regarding new anode materials, zero-strain material $Li_4Ti_5O_{12}$ (LTO) is regarded as a state-of-the-art high power anode due to its long cycle life and high rate capability.[9−11] LTO has a maximum capacity of 175 mAh g^{-1}, which gives an energy density that is insufficient for emerging electrochemical energy storage applications. Niobium-based oxides, whose redox potential window lies between 1.0 and 2.0 V (vs Li/Li^+), have been considered as potential candidates to replace LTO because of their safe lithium insertion potential and high storage capacity at high rates.[12−15] Two kinds of niobium oxides, orthorhombic Nb_2O_5 (T-Nb_2O_5) and monoclinic Nb_2O_5 (H−Nb_2O_5), are commonly used as anode materials for LIBs, which can transfer one-electron per niobium (i.e., Nb^{5+} to Nb^{4+}) in the potential range of 1.2−3.0 V (vs Li/Li^+), resulting in a capacity of ∼200 mAh g^{-1}.[16] When Nb atoms are replaced with Ti atoms, Nb^{5+} can be reduced further to $Nb^{3.5+}$ upon lithiation and yield a reversible capacity up to ∼300 mAh g^{-1}, which is twice the capacity of LTO.[17] In addition, replacing Nb with Ti decreases the price of the material as Ti raw materials are cheaper than Nb raw materials. Toshiba Inc. has recently developed a 49 Ah TNO-based LIB for EV applications with volumetric energy densities of 350 Wh L^{-1} (calculated based on the total weight and volume of a full battery; the comparable energy density of an LTO LIB is 177 Wh L^{-1}) and an input power density up to 10 kW L^{-1} at a 50% state of charge (SOC).[18] In order to fully commercialize TNO anodes, several issues must be addressed.

TNO materials have different compositions and structures that include $TiNb_{24}O_{62}$,[19] $Ti_2Nb_{10}O_{29}$,[20] and $TiNb_2O_7$.[21] Each possess a Roth-Wadsley block oxide structure that differ only by connectivity of each block formed by the presence of shear planes.[17] It is still an active topic of research as to how the differences in each structure facilitate fast Li-ion storage. Recent *in situ* and *operando* characterization techniques have been applied to provide experimental evidence to elucidate the phenomenon.[17,22,23]

Received: August 13, 2020
Revised: September 20, 2020
Published: September 21, 2020

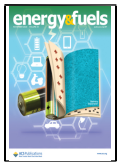

https://dx.doi.org/10.1021/acs.energyfuels.0c02732
Energy Fuels 2020, 34, 13321−13334

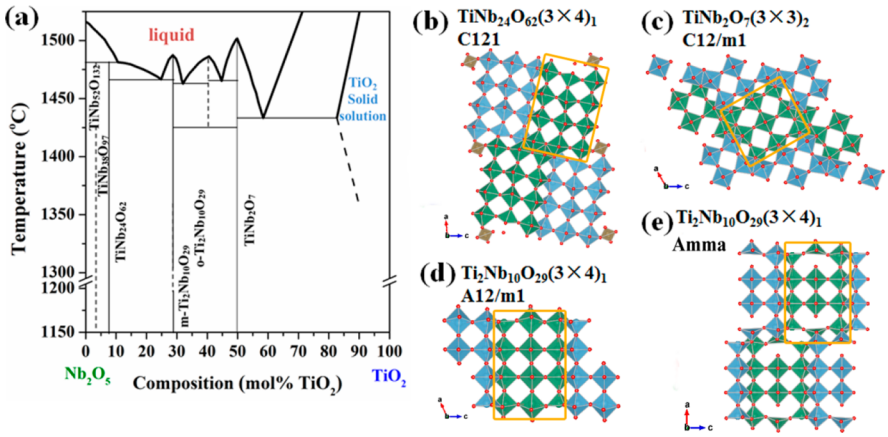

Figure 1. (a) Composition phase diagram of the Nb_2O_5−TiO_2 system at various calcination temperatures. The dashed lines indicate regions where structures are not well-defined,[34,35] and the schematic crystal structures of (b) $TiNb_{24}O_{62}$,[41] (c) $TiNb_2O_7$,[42] (d) monoclinic $Ti_2Nb_{10}O_{29}$,[43] and (e) orthorhombic $Ti_2Nb_{10}O_{29}$[43] (green and blue blocks are offset by 1/2b in the structure).

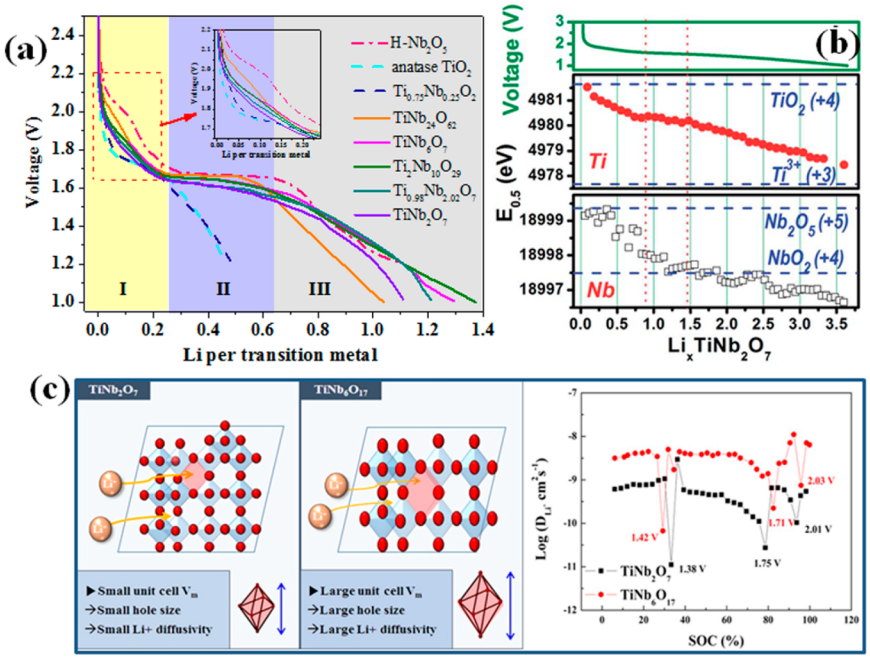

Figure 2. (a) Overlaid profiles of the Li^+ insertion per transition metal (Ti and Nb) behavior for the bulk H−Nb_2O_5,[16] anatase-TiO_2,[46] Nb-doped TiO_2,[46] $TiNb_{24}O_{62}$,[35] $TiNb_6O_{17}$,[37] $Ti_2Nb_{10}O_{29}$,[55] $Ti_{0.98}Nb_{2.02}O_7$,[54] and $TiNb_2O_7$.[54] (b) Valence state variation of Ti and Nb in the $TiNb_2O_7$ anode during the initial discharge estimated from the Ti and Nb XANES edge positions.[53] Reprinted with permission from ref 53. Copyright 2014 The Royal Society of Chemistry. (c) Schematic diagram of phenomena about the unit cell sizes and Li^+ diffusion behaviors of $TiNb_2O_7$ and $TiNb_6O_{17}$ anodes and corresponding Li^+ diffusion coefficients calculated from GITT as a function of the SOC at the charge process.[37] Reprinted with permission from ref 37. Copyright 2017 Nature Publishing Group.

Although TNO anodes have higher theoretical capacities, there are opportunities to further increase the materials capacity and rate performance. For example, by introducing vacancies or heteroatom dopants into TNO, the ionic conductivity can be increased.[24,25] In addition, the electronic conductivity of TNO can also be improved by designing carbons utilizing other conductive materials.[26,27] All of these strategies are beneficial to further increase the (de)lithiation ability of TNO anodes at high current densities.

Although the relatively high redox potential (∼1.65 V vs Li/Li^+) of TNO can prevent the deposition of lithium metal and formation of a thick SEI film on the surface of the anode, the energy density of the cell is decreased as the potential difference between the cathode and anode (calculated using "Ah kg^{-1} ⊆ V" to give units of "Wh kg^{-1}") must be maximized.[28] Therefore, studies related to discharging TNO anodes at lower cutoff potentials, using appropriate high-potential cathodes, and proper full-cell design are currently being performed. Another important problem for TNO full batteries is possible gas evolution. The lack of an SEI film on the surface of TNO anodes can cause degradation of the electrolyte at the TNO/electrolyte interface and result in the evolution of harmful gases.[29,30] Therefore, studies regarding mitigating of gassing will also be discussed in this review.

Finally, recent combinations of TNO anodes with capacitive carbon-based cathodes have been used to construct hybrid lithium-ion capacitors (LICs) that show improvements in power density.[31] This review will discuss pseudocapacitance character-

https://dx.doi.org/10.1021/acs.energyfuels.0c02732
Energy Fuels 2020, 34, 13321−13334

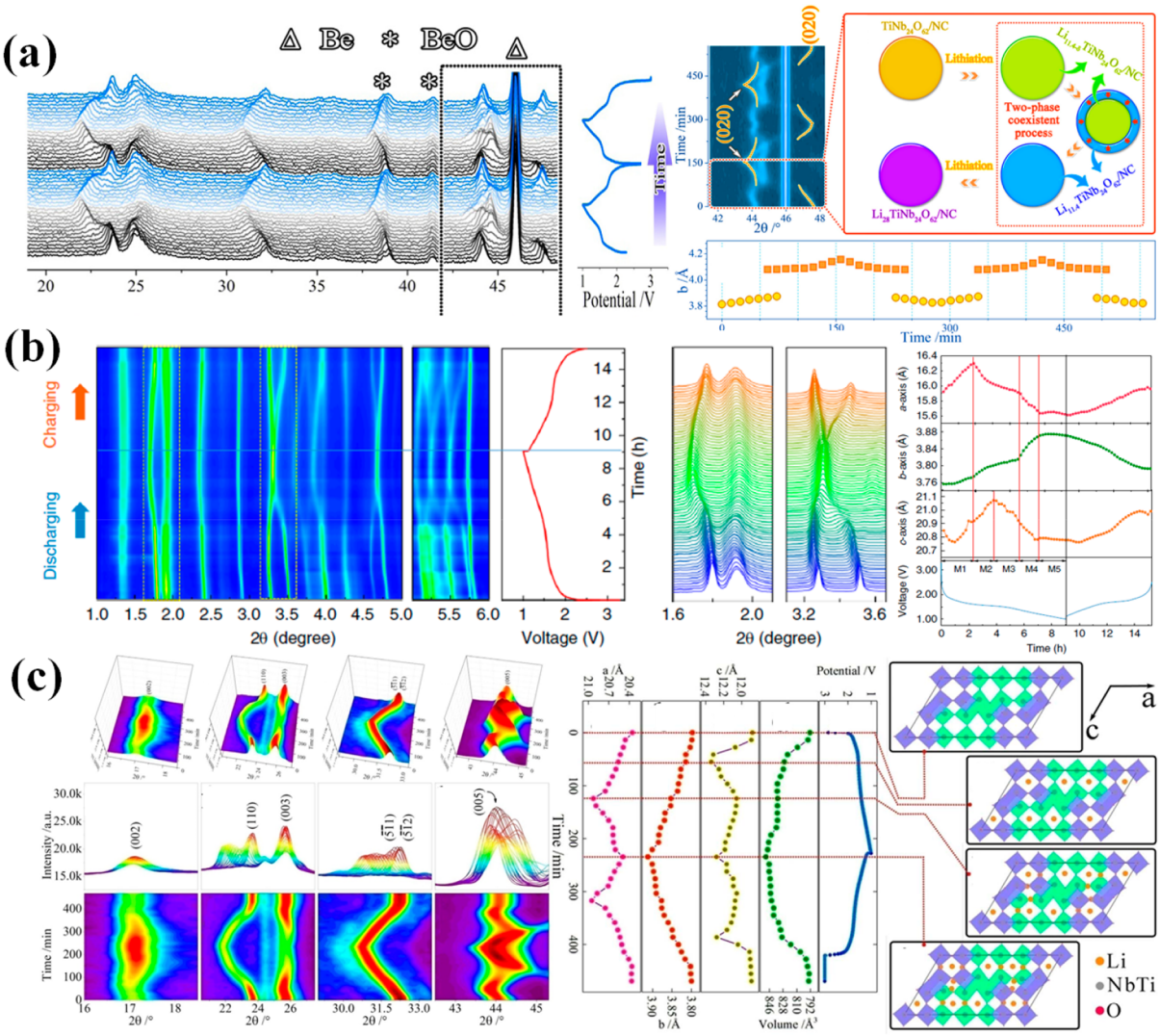

Figure 3. (a) *In situ* XRD patterns of $TiNb_{24}O_{62}$ anode during charge/discharge at 0.45 C and the corresponding change of the lattice parameter *b* from (020) reflection and schematic illustrations of two-phase coexistent reaction for $TiNb_{24}O_{62}$.[17] Reprinted with permission from ref 17. Copyright 2018 Elsevier. (b) *In situ* synchrotron HEXRD characterization voltage profile, corresponding contour plot of the XRD pattern evolution, and the lattice parameter evolution process of $Ti_2Nb_{10}O_{29}$ during the first charge/discharge process.[22] (Reprinted with permission from ref 22. Copyright 2020 Nature Publishing Group. (c) *In situ* XRD patterns of $TiNb_2O_7$ in various 2θ ranges as well as the corresponding lattice parameters, lattice volume changes, and lithiation model at different lithiated/delithiated states.[23] Reprinted with permission from ref 23. Copyright 2017 Elsevier.

istics of TNO anodes and the electrochemical characteristics of the corresponding high-power fuel cells.

2. FUNDAMENTALS OF TNO-BASED MATERIALS

2.1. Crystal Structures of TNO. TNO materials belong to the Wadsley−Roth block structure family, which are oxygen-deficient derivatives of the ReO_3 crystal structure. Ti and Nb atoms are both octahedrally coordinated and are connected by their corners within blocks. Blocks are defined and separated by discrete lines of octahedra that are rotated from corner- to edge-sharing; these lines are called shear planes. Shear planes form in order to compensate for charge imbalance due to oxygen nonstoichiometry.[16] In TNO materials, NbO_6/TiO_6 octahedra provide a 2D interstitial space for Li^+ insertion.[32] The TNO family contains many compositions that vary in terms of the ratio between Ti and Nb. As reported by Eror, the solid-solution limit for Nb in TiO_2 is 8 atom %.[33] Line compounds in the TNO family include $TiNb_{24}O_{62}$, $Ti_2Nb_{10}O_{29}$, $TiNb_6O_{17}$, and $TiNb_2O_7$. The Ti−Nb−O phase diagram is depicted in Figure 1a.[34,35] $TiNb_{24}O_{62}$, $TiNb_2O_7$, and $Ti_2Nb_{10}O_{29}$ can be written in so-called "block notation" as $TiNb_{24}O_{62}(3\times4)_2$, $TiNb_2O_7(3\times3)_\infty$, and $Ti_2Nb_{10}O_{29}(3\times4)_\infty$, where the integers describe the length and width of the blocks in terms of octahedral length in the a−b plane and the subscript describes the connectivity of each block in the c plane (Figure 1b−d).[21] Some TNO compounds such as $Ti_2Nb_{14}O_{39}$ and $TiNb_6O_{17}$ can be considered as monoclinic superstructures containing intergrown phases of $Ti_2Nb_{10}O_{29}$ and Nb_2O_5 with cation vacancies.[36−38] The $Ti_2Nb_{10}O_{29}$ compound has two polymorphs: the monoclinic phase (m-$Ti_2Nb_{10}O_{29}$) that forms below 1200 °C and the orthorhombic phase (o-$Ti_2Nb_{10}O_{29}$) that forms above 1300 °C.[39] Monoclinic $Ti_2Nb_{10}O_{29}$ has been primarily used as an anode for LIBs, while orthorhombic $Ti_2Nb_{10}O_{29}$ has not.[40]

2.2. Lithiation Behavior of TNO. During the lithiation process, it is believed that Nb^{5+} in TNO can be reduced to Nb^{3+} with two electrons transferred per Nb atom.[17] However, recent studies have suggested that in the voltage window from 1.0 to 3.0 V (vs Li/Li^+), Nb^{5+} was not fully reduced to Nb^{3+}. Figure 2a depicts the lithiation behavior of relevant oxides within this voltage window in terms of Li^+ transferred per transition metal in the oxide. It is seen that the lithiation curves of all electrodes can roughly be divided into three regions: *region I*, located between 3 and 1.7 V, that is attributed to the formation of a single solid-

https://dx.doi.org/10.1021/acs.energyfuels.0c02732
Energy Fuels 2020, 34, 13321−13334

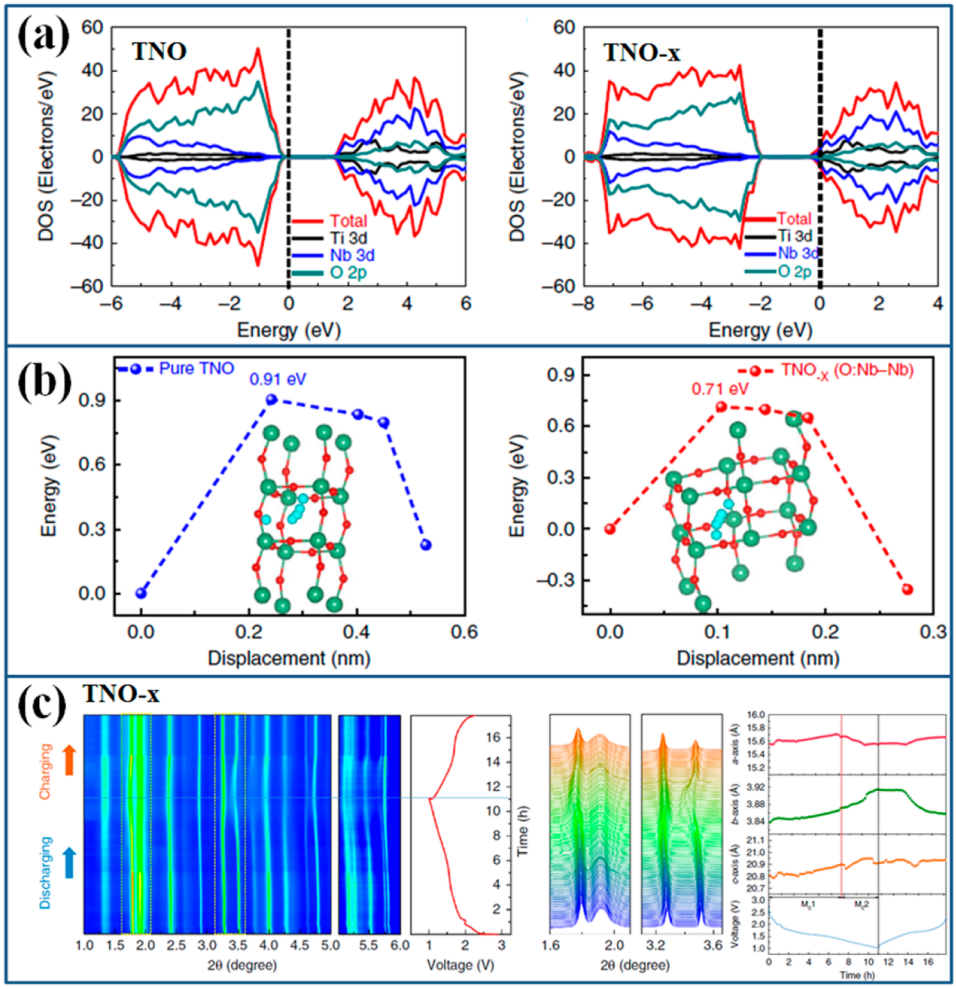

Figure 4. Comparison of (a) density of states (DOS) and (b) Li-ion diffusion energy barrier of pure $Ti_2Nb_{10}O_{29}$ and defective $Ti_2Nb_{10}O_{29-x}$. (c) *In situ* synchrotron HEXRD characterization voltage profile, corresponding contour plot of the XRD pattern evolution, and the lattice parameter evolution process of the defective $Ti_2Nb_{10}O_{29-x}$ sample during the first charge/discharge process.[22] Reprinted with permission from ref 22. Copyright 2020 Nature Publishing Group.

solution phase; *region II*, located between 1.7 and 1.6 V, a constant voltage plateau that corresponds to the existence of the two-phase region; and *region III*, located between 1.6 and 1 V, which is attributed to the formation of another solid solution.[44] Anatase-TiO_2 possesses a ReO_3 structure with corner/edge sharing TiO_6 octahedra[45] that can accommodate 0.5 Li per Ti atom in the potential range of 3−1.2 V.[46] If 25 atom % Nb^{5+} is added to anatase-TiO_2, Li^+ insertion rates increase due to lattice expansion (the Scherrer crystallite sizes increase from 4.3 to 5.0 nm after doping).[46,47] A similar phenomenon is seen in Ti-doped Nb_2O_5.[48] The presence of both TiO_6/NbO_6 octahedra promotes structural defects that facilitate the diffusion of Li^+.[48,49]

H−Nb_2O_5 and TNO compounds exhibit a shoulder subplateau between 1.90 and 2.05 V in region I (Figure 2a). It is believed that this small subplateau of TNO compounds is ascribed to the reduction of $Ti^{4+} \rightarrow Ti^{3+}$.[24,50−52] However, because the subplateau exists in H−Nb_2O_5, this mechanism might not be correct. Guo et al.[53] showed using X-ray absorption near edge spectroscopy (XANES) that the reductions of Ti^{4+} and Nb^{5+} in TNO start simultaneously and proceeds equivalently during discharge (Figure 2b). The subplateaus in region I become obscured with increasing Ti content (inset in Figure 2a). The amount of Li^+ intercalation is not directly proportional to the proportion of Ti atoms in the active TNO compounds even if the selected systems in Figure 2a are all bulk morphologies. Both $TiNb_6O_{17}$ and $Ti_2Nb_{10}O_{29}$ exhibit more Li-insertion than $TiNb_2O_7$ in the same discharge potential range. Lee et al.[37] showed that $TiNb_6O_{17}$ has better lithium diffusion kinetics than $TiNb_2O_7$ due to a larger unit cell volume and more available Li^+ insertion sites (Figure 2c). $Ti_{0.98}Nb_{2.02}O_7$ has higher rate performance than pure $TiNb_2O_7$ due to the narrowed band gap.[54]

Recent *operando* studies provide more detail about charge storage mechanisms in TNO materials. Figure 3 shows data gathered using *operando* XRD that allows for the quantification of the lattice parameter evolution during Li-ion insertion/extraction into/from $TiNb_{24}O_{62}$,[17] $Ti_2Nb_{10}O_{29}$,[22] and $TiNb_2O_7$[23] materials. For $TiNb_{24}O_{62}$, as shown in Figure 3a, Li^+ is first intercalated into the lattice along the *b* axis to randomly occupy sites located at the face center of Nb(Ti)O cubes, resulting in an increase in the length of the *b* axis.[17] In region I, Li ions diffuse rapidly in tunnels along the *b* axis. Griffith et al.[21] showed that Li^+ diffusion in $TiNb_2O_7$ is anisotropic with activation barriers of 100−200 meV down tunnels and 700−1000 meV across blocks. After the insertion amount of lithium reaches ∼0.5 Li^+ per transition metal (after region I in Figure 2a), the lattice parameter along the *b* axis expands significantly, indicating that lithium occupies spaces between lattice planes perpendicular to the *b* axis. Deng et al.[22] measured the lattice evolution during initial lithiation of $Ti_2Nb_{10}O_{29}$ by in situ synchrotron high-energy synchrotron X-ray diffraction (HEXRD; Figure 3b). The study found that initial structural transformation of $Ti_2Nb_{10}O_{29}$ in the potential window 3.0−1.5 V (vs Li/Li^+) was irreversible. The transformation involved a permanent *a*- and *c*-axis expansion. Similar to $TiNb_{24}O_{62}$, the *b* axis expands after the two-phase reaction (discharge plateau). A similar phenomenon occurs in $TiNb_2O_7$ with a different *a*/*c*-axis expansion (Figure 3c).[23] The expansion of the *b* axis

https://dx.doi.org/10.1021/acs.energyfuels.0c02732
Energy Fuels 2020, 34, 13321−13334

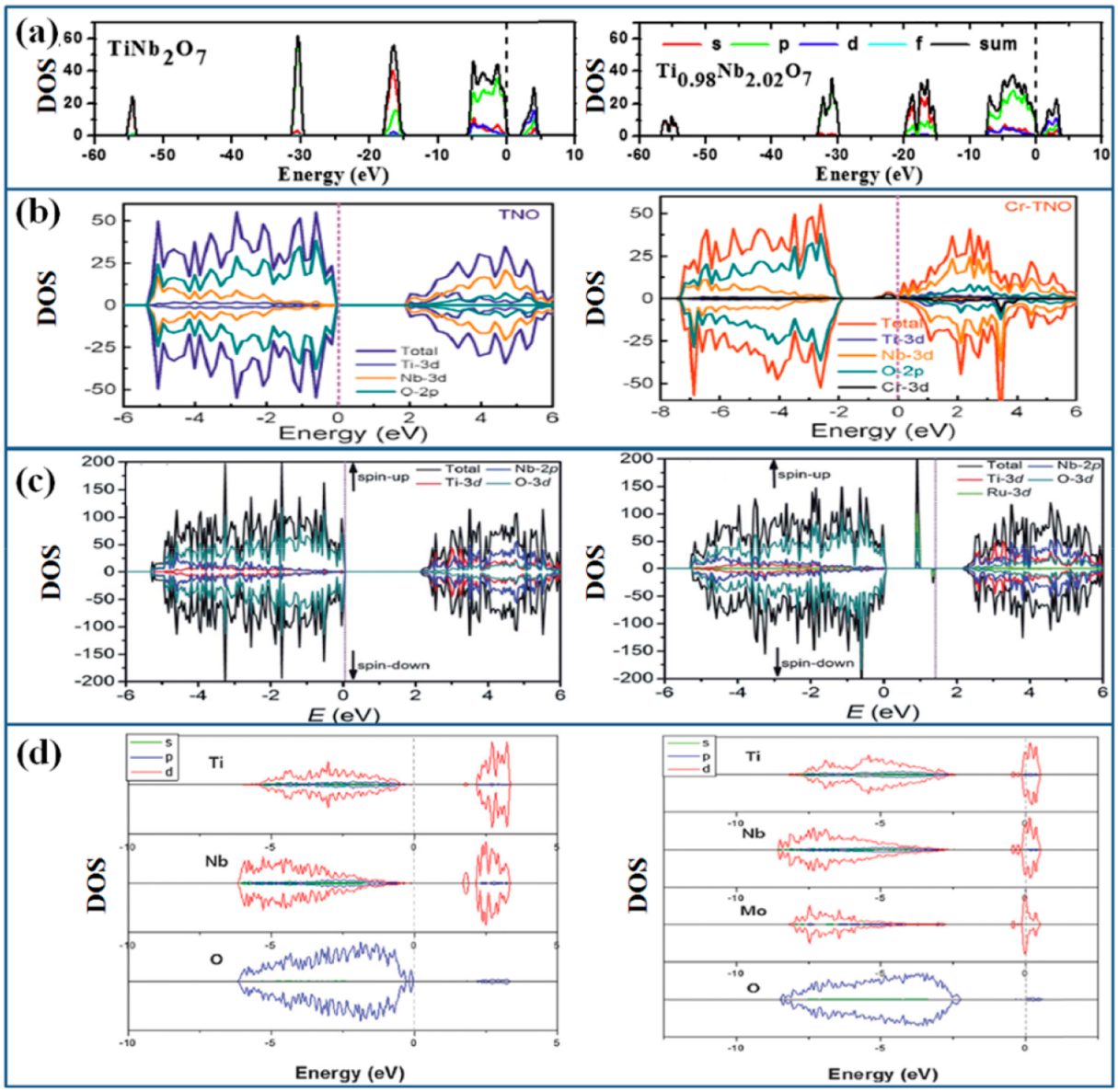

Figure 5. Calculated density of states (DOS) of (a) $TiNb_2O_7$ and $Ti_{0.98}Nb_{2.02}O_7$.[54] Reprinted with permission from ref 54. Copyright 2017 Elsevier. (b) $Ti_2Nb_{10}O_{29}$ and Cr-doped $Ti_2Nb_{10}O_{29}$.[69] Reprinted with permission from ref 69. Copyright 2020 Wiley. (c) $TiNb_2O_7$ and $Ru_{0.01}Ti_{0.99}Nb_2O_7$.[70] Reprinted with permission from ref 70. Copyright 2015 The Royal Society of Chemistry. (d) $TiNb_2O_7$ and Mo-doped $TiNb_2O_7$ (left, pristine TNO; right, doped-TNO).[72] Reprinted with permission from ref 72. Copyright 2015 The Royal Society of Chemistry.

is linear with the amount of inserted Li^+ irrespective of the ratio of Ti/Nb.[56] The unit-cell volume expands by 6−9% for $TiNb_2O_7$ and $Ti_2Nb_{10}O_{29}$ and more than 17% for $TiNb_{24}O_{62}$.[17,23,44,53,56−58] This is larger than the expansion experienced by $Li_4Ti_5O_{12}$ (less than 1% between $Li_4Ti_5O_{12}$ and $Li_7Ti_5O_{12}$).[9,10] It is understood that smaller unit-cell volume changes during lithiation enable more stable cycling. Therefore, efforts such as introduction of oxygen defects, doping of metal ions, and large-scale structural design have been studied in order improve the rate performance of TNO anodic materials.

3. STRATEGIES FOR IMPROVEMENT OF PERFORMANCE

TNO materials are considered promising anode candidates to replace $Li_4Ti_5O_{12}$ as power supplies for EVs, HEVs, and other high-power applications due to higher theoretical capacities owing to the multiple redox couples of Ti^{4+}/Ti^{3+}, Nb^{5+}/Nb^{4+}, and Nb^{4+}/Nb^{3+}. Actual reversible capacities based on these redox couples are hard to access in the voltage range of 1−3 V (vs Li/Li^+).[59,60] The large volume expansion of TNO materials will degrade cycle performance over continued cycles. Strategies to address these issues include defective structure design, elemental doping, composite design with conductive materials and other active materials with high lithiation capacities, and overlithiation by reducing discharge potential. The specific modification approaches and the corresponding lithiation/delithiation mechanisms are summarized below.

3.1. Structure Design with Oxygen Vacancies. As early as 2006, Sheppard et al.[61] studied the influence of defects on the conductivity of Nb doped TiO_2 by measuring the conductivity of reduced Nb-doped TiO_2. The equilibrium constant for the formation of oxygen and Ti vacancies as well as the effect of Nb on this constant was quantified. They found that under reducing atmospheres, the electronic structure of Nb-doped TiO_2

https://dx.doi.org/10.1021/acs.energyfuels.0c02732
Energy Fuels 2020, 34, 13321−13334

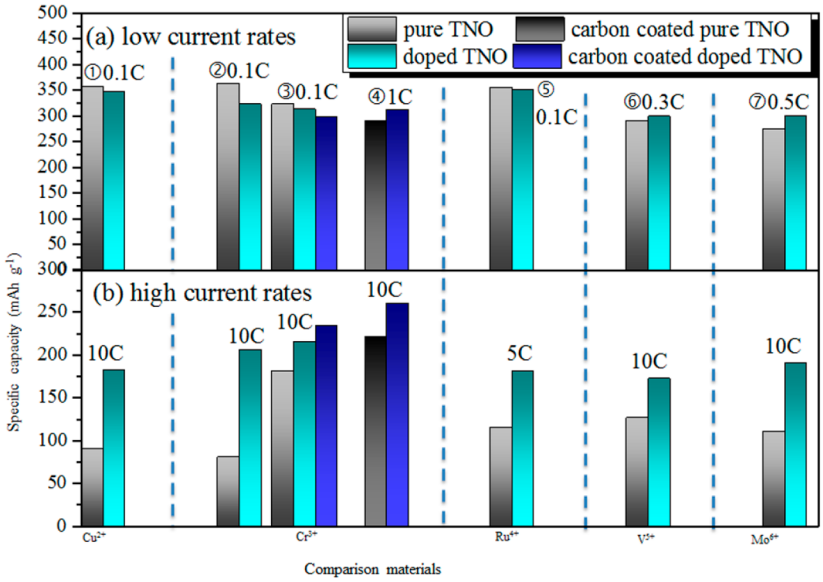

Figure 6. Specific capacities comparison of pristine TNO and various metal-ion doped TNO materials at (a) low and (b) high current rates. The comparative modified materials from left to right are as follows: (1) $Cu_{0.02}Ti_{0.94}Nb_{2.04}O_7$,[67] (2) $Cr_{0.6}Ti_{0.8}Nb_{10.6}O_{29}$,[25] (3) $Cr_{0.5}TiNb_{10.5}O_{29}$/CNT,[68] (4) Cr−$Ti_2Nb_{10}O_{29}$@VGTC,[69] (5) $Ru_{0.01}Ti_{0.99}Nb_2O_7$,[70] (6) $TiNb_{1.98}V_{0.02}O_7$,[71] and (7) Mo-$TiNb_2O_7$.[72]

underwent a sudden change from semiconducting to metallic-type conduction. The mechanism of this transition was attributed to structural changes leading to either a Mott-type or defect-driven Anderson-type metal−insulator transition.[61] Zhai et al.[48] reported that the conductivity and electrochemical reaction activity of Ti-doped Nb_2O_5 can also be improved by the introduction of oxygen vacancies. Oxygen vacancies have been observed to introduce impurity energy levels in the bandgap and increase the corresponding electrical conductivity.[62] Therefore, structure design by tuning oxygen vacancies in the TNO structures is a suitable method to improve their intrinsic electronic conductivity. Oxygen defects can be introduced by annealing TNO precursors either under a vacuum, inert or reducing atmosphere,[24,63−65] or by calcination with reducing agents.[22,66] Inada et al.[63] reported that the color of a vacuum-annealed $TiNb_2O_7$ material changed from white to dark blue. A similar phenomenon has been seen for H−Nb_2O_5 materials. Li et al.[67] observed that when H−Nb_2O_5 was reduced to $Nb_{25}O_{62}$, the color of the sample changed from white to mazarine blue. This color change can be attributed to the production of Nb^{4+} ions in the reduced TNO samples.[67]

Deng et al.[22] investigated the electronic structure, Li^+ diffusion, and structural stability of oxygen defective $Ti_2Nb_{10}O_{29-x}$ by DFT calculations and *operando* synchrotron HEXRD characterization. The densities of state (DOSs) of pure $Ti_2Nb_{10}O_{29}$ and oxygen defective $Ti_2Nb_{10}O_{29-x}$ are shown in Figure 4a. The Fermi level shifts from the top of the valence band for pure $Ti_2Nb_{10}O_{29}$ to the bottom of the conduction band for oxygen defective $Ti_2Nb_{10}O_{29-x}$, implying that $Ti_2Nb_{10}O_{29}$ experiences metallic-like conductivity through the introduction of oxygen vacancies. Conduction band peaks of defective $Ti_2Nb_{10}O_{29-x}$ cross the Fermi level, indicating the enhancement of the intrinsic electronic conductivity of oxygen defective samples.

It has been reported that the electronic conductivity of pure $TiNb_2O_7$ will increase by 7 orders of magnitude upon lithiation.[21] Therefore, another theory suggests that oxygen vacancies improve Li^+ diffusivity and buffer unit-cell volume changes during lithiation. As shown in Figure 4b, the calculated Li^+ diffusion energy barrier of pure $Ti_2Nb_{10}O_{29}$ is 0.91 eV. When oxygen vacancies are introduced, the barrier decreases to 0.71 eV.[22]

When Li^+ is inserted into TNO, the host atoms rearrange to tolerate Li insertion. In situ XRD results shown in Figure 4c demonstrate that with the introduction of oxygen vacancies in $Ti_2Nb_{10}O_{29-x}$, lattice anisotropy was decreased compared to pure $Ti_2Nb_{10}O_{29}$ (Figure 3b). The introduction of oxygen defects can alleviate structural distortion of TNO during lithiation. Correspondingly, the cyclic stability and rate capacities of TNO_{-x} can be improved.[22]

3.2. Elemental Doping. Elemental doping is another method for enhancing the intrinsic electronic/ionic conductivity of TNO materials. In essence, elemental doping may also introduce defects into the TNO structure. Several studies have demonstrated improved electrochemical performance of TNO from dopants with oxidation states varying from +2 (Cu^{2+}) to +6 (Mo^{6+}).[25,67−72] When doping lower valence states ions (such as Cu^{2+} and Cr^{3+}) into the TNO structure, excess Nb^{5+} is required to maintain charge balance.[25,67]

The representative densities of state (DOSs) for pristine and Nb^{5+}, Cr^{3+}, Ru^{4+}, and Mo^{6+} doped $TiNb_2O_7$ are shown in Figure 5.[54,69,70,72] Figure 5a shows that by changing the amount of Nb by 2%, the band gap of $Ti_{0.98}Nb_{2.02}O_7$ narrows due to energy level splitting.[54] The Fermi level did not shift after increasing the amount of Nb. If Ti or Nb atoms are replaced with atoms such as Cr^{3+}, Ru^{4+}, and Mo^{6+}, depicted in Figure 5b−d, the Fermi level shifts and the character of the conductivity changes from insulating to metallic. A difference in valence state between dopants and either Ti^{4+} or Nb^{5+} causes the Fermi level to shift from the top of the valence band to the bottom of the conduction band,[69,72] which is indicative of a change from p-type to n-type conductivity after doping. The electron conductivity of doped samples is improved due to the presence of impurity levels in the band gap. If the valence state of the dopants is the same as that of either Nb^{5+} or Ti^{4+}, the Fermi level will shift to the middle of the valence band and conduction band,

https://dx.doi.org/10.1021/acs.energyfuels.0c02732
Energy Fuels 2020, 34, 13321−13334

and some impurity bands will appear close to the Fermi level. This effect can be attributed to the hybridization of the orbitals of the dopant and oxygen, which is seen in the case of Ru^{4+} doping where Ru 4d and O 2p hybridize.[70]

Doping ions with a larger radius (e.g., Cu^{2+},[67] Cr^{3+},[25] Ru^{4+},[70] Mo^{6+},[72] etc.) can increase the volume of the unit cell of TNO. Cr^{3+} and Nb^{5+} codoped $Cr_{0.6}Ti_{0.8}Nb_{10.6}O_{29}$, where Cr^{3+}/Nb^{5+} are larger in size (0.64/0.615 Å) compared with Ti^{4+} ions (0.605 Å), showed an increase in unit cell volume of ~0.6% (1124.31 ± 0.14 Å^3) compared to pristine $Ti_2Nb_{10}O_{29}$ (1117.67 ± 0.15 Å^3). Song et al.[73] proposed that the Li^+ diffusion coefficient can be increased by 1 to 3 orders of magnitude when the unit cell volume expands by 1%. Therefore, $Cr_{0.6}Ti_{0.8}Nb_{10.6}O_{29}$ possesses more suitable Li^+ diffusion pathways in the host materials, resulting in a larger Li^+ diffusion coefficient of 1.42×10^{-14} cm^2 s^{-1} than that of the pristine $Ti_2Nb_{10}O_{29}$ sample (1.55×10^{-15} cm^2 s^{-1}).

The specific capacities of pristine TNO materials and corresponding doped samples at low and high rates are depicted in Figure 6. In Figure 6a, pristine TNO materials exhibit similar or higher specific capacity compared to doped samples at low current rates below 1 C. With increasing the rates to 5 or 10 C, doped samples show higher capacities than pristine TNO materials due to better intrinsic ionic and electronic conductivity (Figure 6b). Both pure TNO and doped-TNO with carbon coating have higher capacities than those without carbon coating. Multiple optimization conditions (e.g., doping, carbon coating, etc.) fully maximize the rate performance of TNO materials.

3.3. Composite Design. To facilitate ion/electron transfer from the TNO/electrolyte interface, within TNO materials, and finally to the current collector, electrically conductive TNO composites must be designed. Typical TNO composites are shown in Figure 7a. Materials combined with TNO can be divided into carbon, metal, or semiconductor material composites,[24,27,51,74] Ti/Nb oxide self-dopants to improve the ionic conductivity,[75] materials with strong mechanical stability to stabilize the structure change during the Li^+ insertion/extraction process,[76] and other anodic materials with high capacities to increase the lithiation capacities.[77] Combining two or more materials with TNO is a promising strategy to improve the electrochemical performance of TNO.[51,66,76,78]

3.3.1. Carbon-Based Composites. Advanced carbonaceous materials, such as carbon nanofibers (CNFs),[74] carbon nanotubes (CNTs),[26,79] ketjen black (KB),[26] graphene,[78] bacterial cellulose carbon (BCC),[24] activated carbon cloth (ACC),[80] carbon nanosheets (CNSs),[66] and heteroatom-doped amorphous carbon from polymer pyrolysis,[81,82] are common materials to improve the cycling stability and rate capability of TNO composites. Carbon can not only increase the electronic conductivity of TNO materials but can also reduce TNO and form oxygen vacancies, further increasing the ionic conductivity of TNO materials.[66,83]

There are two main types of carbon sources, inorganic carbon sources and organic carbon sources. For some advanced inorganic carbon sources, such as one-dimensional (1D) carbon fibers,[66,80] CNFs,[74] CNTs,[26] and BCC[24] as well as two-dimensional (2D) graphene[78] and CNSs,[66] conductive carbon frameworks are formed by self-assembly, and then TNO nanoparticles are grown on the surface of the carbon framework under a solvothermal or hydrothermal reaction to form TNO/C composites. Organic carbon sources, such as polydopamine,[78] polyimide,[81] ethylenediamine tetraacetic acid (EDTA),[17] etc.,

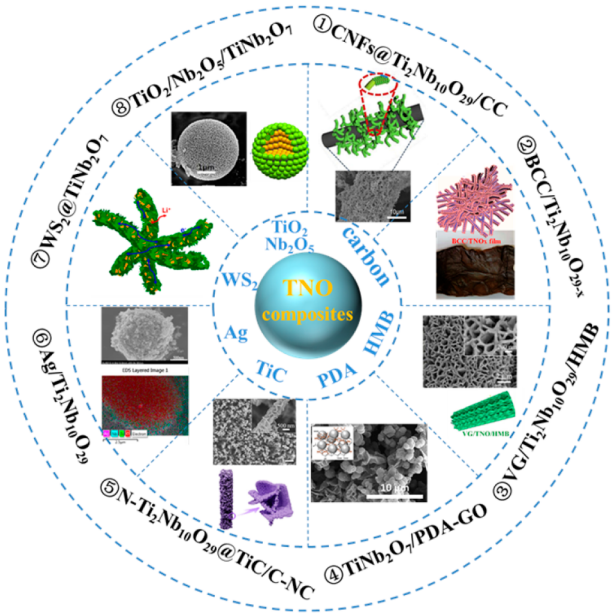

Figure 7. Morphologies and structural diagrams of typical TNO based composites: (1) CNFs@$Ti_2Nb_{10}O_{29}$/CC[74] (Reprinted with permission from ref 74. Copyright 2020 Elsevier). (2) CC/$Ti_2Nb_{10}O_{29-x}$[24] (Reprinted with permission from ref 24. Copyright 2019 Elsevier). (3) Vertical graphene/$Ti_2Nb_{10}O_{29}$/HMB[51] (Reprinted with permission from ref 51. Copyright 2018, Elsevier). (4) $TiNb_2O_7$/polydopamine-GO[78] (Reprinted with permission from ref 78. Copyright 2020 Wiley). (5) N−$Ti_2Nb_{10}O_{29}$@TiC/C-NC[66] (Reprinted with permission from ref 66. Copyright 2020, Elsevier). (6) Ag/$Ti_2Nb_{10}O_{29}$[27] (Reprinted with permission from ref 27. Copyright 2020 World Scientific Publishing Company). (7) WS_2@$TiNb_2O_7$[77] (Reprinted with permission from ref 77. Copyright 2019 The Royal Society of Chemistry). (8) $TiO_2/Nb_2O_5/TiNb_2O_7$[75] (Reprinted with permission from ref 75. Copyright 2017 Elsevier).

are usually coated on the surface of the prepared TNO particles by pyrolysis. If there are heteroatoms in the organic carbon source, the heteroatoms will be doped into the carbon layer or even TNO structure during pyrolysis. Yu et al.[17] compared the carbon-coating modified $TiNb_{24}O_{62}$ with EDTA and glucose as organic carbon sources. EDTA-based carbon coating caused considerable nitrogen doping where $TiNb_{24}O_{62}$/NC electrodes showed faster dynamic characteristics than $TiNb_{24}O_{62}$/C (the carbon derived from glucose pyrolysis). The discharge capacity of $TiNb_{24}O_{62}$/NC was 181.8 mAh g^{-1} at 5 C while $TiNb_{24}O_{62}$/C electrode exhibited 157.0 mAh g^{-1} at the same C rate.

The rate performances of before and after modified TNO/C composites reported in recent years within the charge/discharge range of 1−3 V are compared in the form of a boxplot in Figure 8.[17,22,24,26,51,66,69,74,78,81−86] The highest capacities (graphene/$Ti_2Nb_{10}O_{29}$/hydrogen molybdenum bronze (HMB) and TNO@N−C) can exceed 300 mAh g^{-1} even at a discharge rate of 5 C.[51,81] At a current rate of 40 C, the capacity of the N-TNO@TiC/C-NC sample can reach 225 mAh g^{-1}.[66] This indicates that the combination of various modification methods can lead to better electrochemical performance. Considering the average rate capacities of pristine and carbon modified TNO composites shown in the inserted table in Figure 8, carbon modified TNO shows higher rate capacities than that of the pristine materials. The average capacity of modified TNO/C is 50% higher than that of pristine TNO at 40 C.

https://dx.doi.org/10.1021/acs.energyfuels.0c02732
Energy Fuels 2020, 34, 13321−13334

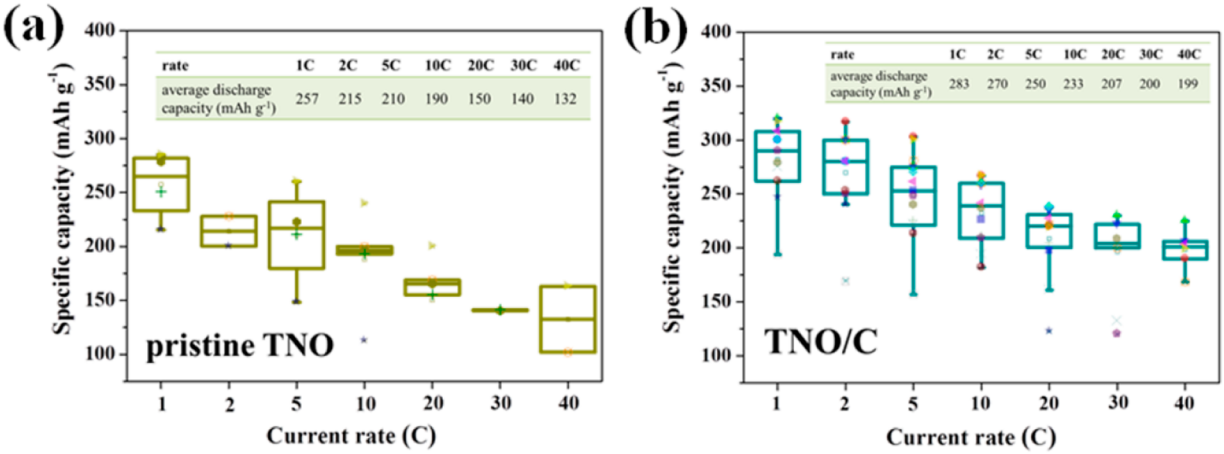

Figure 8. Boxplot of rate performances of (a) before and (b) after carbon modified TNO/C composites reported in the past three years (inserted table: the average rate discharge capacities).

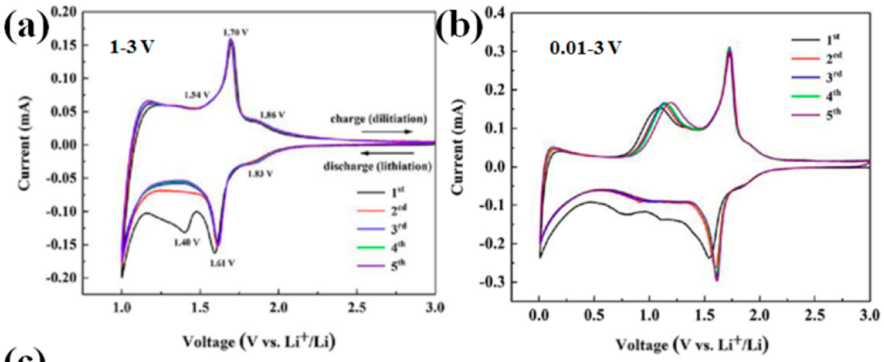

(c)

Voltage window (V)	Initial discharge capacity (mAh g-1)	Initial charge capacity	Initial coulombic efficiency	Discharge capacity after 100 cycles	Capacity retention rate after 100 cycles
1.0-3.0 V	376	330	87.0 %	315	83.7 %
0.01-3.0 V	414	348	84.0 %	320	74.4 %

Figure 9. CV curves of the ACC@$TiNb_2O_7$ electrode at 0.1 mV s^{-1} from (a) 1.0 to 3.0 V and (b) 0.01 to 3.0 V (vs Li/Li^+). (c) The comparison electrochemical performance data of the ACC@$TiNb_2O_7$ composite in different voltage windows.[80] Reprinted with permission from ref 80. Copyright 2020 Elsevier.

3.3.2. Non-Carbon Based Composites. In addition to carbon materials, other materials, such as highly conductive metal (e.g., silver),[27,87] semiconductors (e.g., HMB),[51] self-dopants (i.e., Ti/Nb oxide),[75] ceramic material (e.g., titanium carbide (TiC)),[76,84] other anodic materials (e.g., WS_2, MoS_2),[77,88] etc., have been used in combination with TNO.

Among them, silver, a highly conductive metal, has often been combined with oxide anode materials to increase the electronic conductivity of the materials.[89,90] However, although the conductivity of silver is higher than that of carbon, silver is heavy and costly, limiting its commercial viability. In addition, some n-type semiconductor materials, such as HMB (electrical conductivity of 103−105 S m^{-1} and ionic conductivity of 10^{-2} S m^{-1}) have been used to improve the electronic conductivity of TNO.[51] Deng et al. designed a vertical graphene/$Ti_2Nb_{10}O_{29}$/HMB composite. The optimal material exhibited a rate capacity of 163 mAh g^{-1} at 60 C, which is superior to the vertical graphene/$Ti_2Nb_{10}O_{29}$ counterpart (124 mAh g^{-1} at 60 C).[51]

Previously, it was shown that impure phases (such as anatase/rutile TiO_2) in the structure of $Li_4Ti_5O_{12}$ can improve its electrochemical performance through interfacial pseudocapacitance between $Li_4Ti_5O_{12}$ and impurity phases.[10] This principle is also applicable to TNO. Wang et al.[75] prepared a mesoporous spherical $TiO_2/Nb_2O_5/TiNb_2O_7$ composite with interconnected TiO_2, Nb_2O_5, and $TiNb_2O_7$ nanocrystals that shorten Li^+ diffusion pathways and provide interconnected channels for fast electron transport. The reversible discharge capacity of the multiphase Ti−Nb oxides is 185.3 mAh g^{-1} at 5 C, with a capacity fade of 5.3% after 1800 cycles.

TiC not only has the rigidity of ceramic materials but also possesses excellent conductive properties, making it an ideal conductive framework to achieve rapid dynamic processes in various electrochemical energy storage systems.[91−93] TiC has been used as a support for TNO[84] and as a surface coating.[76] Luo et al. prepared a single-core/dual-shell m-TNO@TiC@NC composite and found that the m-TNO@TiC@NC composite

https://dx.doi.org/10.1021/acs.energyfuels.0c02732
Energy Fuels 2020, 34, 13321−13334

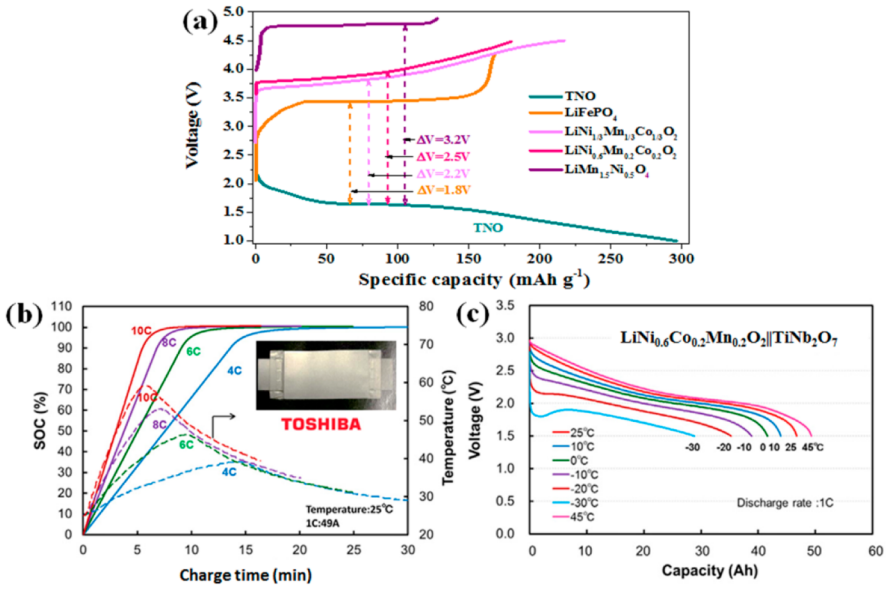

Figure 10. (a) Typical discharge curve of TNO anode and charge curves of various cathodes and the performance of 49 Ah $LiNi_{0.6}Co_{0.2}Mn_{0.2}O_2$||$TiNb_2O_7$ pouch fuel cell prepared by Toshiba Inc. (b) Discharge voltage curves at various temperatures. (c) Changes in SOC (solid line) and battery temperature (dashed line) at various rates.[18] Reprinted with permission from ref 18. Copyright 2018 Elsevier.

has a high capacity of 328.6 mAh g^{-1} at 0.5 C after 200 cycles in the voltage range of 0.01−3 V.[76]

Composites using high capacity anodic materials such as metal sulfides can improve the specific discharge capacity of TNO.[77,88] WS_2@$TiNb_2O_7$ exhibited a reversible rate discharge capacity of 627 mAh g^{-1} at 1 A g^{-1} after 200 cycles and 344 mAh g^{-1} at 5 A g^{-1} after 300 cycles.[77] The $TiNb_2O_7$@MoS_2/C composite obtained a reversible discharge capacity of 531.5 mA h g^{-1} at 0.5 A g^{-1} and 286.6 mA h g^{-1} at a current density of 5 A g^{-1}.[88] But it is worth noting that the voltage range of these composites is wider than typical for TNO, ranging from 0.01 to 3.0 V (vs Li/Li$^+$).

3.4. Over-Lithiation at Low Potentials. At a cutoff voltage above 1.0 V (vs Li/Li$^+$), the formation of an SEI can be avoided to some extent. Ti^{4+} is continuously reduced to Ti^{3+} in the range of 3.0 to 1.0 V. Nb^{5+} is reduced to Nb^{4+} from 3.0 to 1.6 V then to Nb^{3+} from 1.6 to 1.0 V.[17,60] Some researchers have reduced the cutoff potential to 0.01 V (vs Li/Li$^+$) in order to make full use of composite active materials with the capability to store Li below 1.0 V.[76,77,80,88] Luo et al. compared the performance of activated carbon cloth supported $TiNb_2O_7$(ACC@$TiNb_2O_7$) using different voltage windows.[80] CV results shown in Figure 9a and b show a rectangular area below 1.0 V. The authors believe this portion is due to insertion/extraction into/from the activated carbon cloth. From a comparison of electrochemical performance data in different voltage windows (Figure 9c), it is seen that the high capacity contributed by discharging to 0.01 V (vs Li/Li$^+$) results in a sacrifice of initial Coulombic efficiency and rapid capacity decay. The decrease in stability is likely due to large volume changes from overlithiation that leads to irreversible structure change.[80]

4. IMPROVEMENTS IN TNO ANODE-BASED FULL CELLS

Although TNO has a higher volumetric capacity than graphite, the high working potential results in a loss in specific energy density. Therefore, a high-voltage cathode is required to compensate for the narrow voltage window of TNO materials. In order to make full use of the high-rate capability of TNO anode materials, a high-rate cathode or new high-power energy storage devices must be designed. Hybrid ion capacitors are promising devices for fast energy storage because they combine the merits of both supercapacitors and LIBs.[94,95] LIBs typically have a high energy density of 120−200 Wh kg^{-1} but relatively low power density and short cycle life. Supercapacitors possess high power densities of 2−5 kW kg^{-1} and outstanding cycle performance but very low energy densities (2−5 Wh kg^{-1}).[94] LICs couple an intercalation-based anode with a high rate surface-adsorption based cathode to combine the merits of both LIBs and supercapacitors and to deliver high energy and power densities simultaneously.[96] Due to rapid Li$^+$ intercalation/deintercalation in TNO materials, there is interest in using the material as an anode for asymmetric LICs.

4.1. TNO-Based LIBs. *4.1.1. Full-Batteries Design.* Goodenough et al. reported a 3 V fuel cell with carbon-coated $TiNb_2O_7$ as the anode and spinel $LiNi_{0.5}Mn_{1.5}O_4$ as the cathode.[32] TNO anodes have been combined with numerous cathode materials to build batteries possessing high energy/power density, safety, and stability. The reported cathodes include layered oxides ($LiNi_{1/3}Mn_{1/3}Co_{1/3}O_2$,[29] $LiNi_{0.6}Mn_{0.2}Co_{0.2}O_2$,[18,82] $LiNi_{1/3}Mn_{1/3}Co_{1/3}O_2$ + $LiNi_{0.5}Mn_{0.5}O_2$[97]), spinel ($LiMn_{1.5}Ni_{0.5}O_4$[29,32]), and olivine-type materials ($LiFePO_4$[17,30,51]). As shown in Figure 10a, delithiation potentials and specific capacities of each cathode material are different. The spinel $LiMn_{1.5}Ni_{0.5}O_4$ has the highest lithiation/delithiation potential of 4.8 V (vs Li/Li$^+$). The $LiMn_{1.5}Ni_{0.5}O_4$||TNO fuel cell has an average voltage of 3.2 V. The poor stability and rate performance of $LiMn_{1.5}Ni_{0.5}O_4$ cathodes limit performance of the fuel cell.[98] Buannic et al.[29] assembled 11 mAh pouch fuel cells combining nano-$TiNb_2O_7$ with $LiMn_{1.5}Ni_{0.5}O_4$. The system delivered suitable capacities at 0.1 C but experienced rapid capacity fading at rates above 1 C. This inferior electrochemical performance was mainly caused by the electrochemical instability of the $LiMn_{1.5}Ni_{0.5}O_4$ cathode and corresponding swelling behavior of the $TiNb_2O_7$//

https://dx.doi.org/10.1021/acs.energyfuels.0c02732
Energy Fuels 2020, 34, 13321−13334

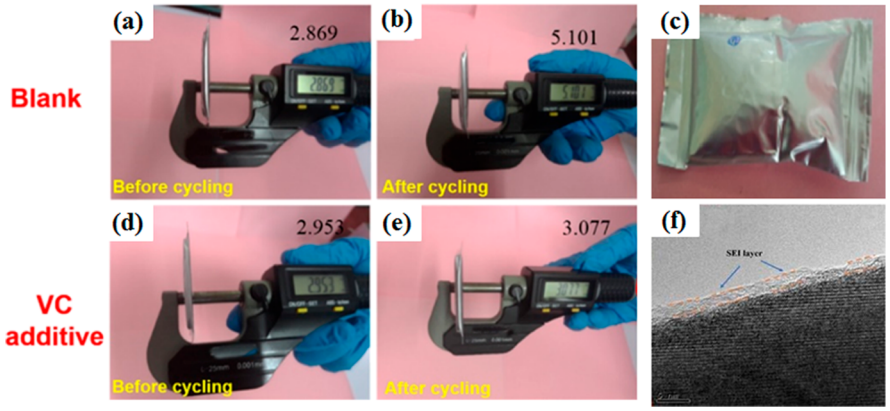

Figure 11. Thickness comparisons of the $LiFePO_4$||$TiNb_2O_7$ pouch fuel cell before and after 250 cycles: (a,b) without VC additive, (d,e) with VC additive, and (c) swell phenomenon of $LiFePO_4$||$TiNb_2O_7$ pouch cell without VC additive after 300 cycles at 1 °C with operation temperature of 40 °C. (f) TEM image of the $TiNb_2O_7$ anode after three cycles in the electrolyte with VC additive.[30] Reprinted with permission from ref 30. Copyright 2018 American Chemical Society.

$LiMn_{1.5}Ni_{0.5}O_4$ fuel cell, which will be described in detail in the Gassing Issues section.

When olivine-structured $LiFePO_4$ is used as a cathode, fuel cells show improved safety, power, and cycling stability. Yu et al.[17] assembled a fuel cell with $TiNb_{24}O_{62}$/NC as an anode and $LiFePO_4$ as a cathode. The fuel cell delivered an initial discharge capacity of 112.7 mAh g^{-1} at a current rate of 1 C and maintained a capacity of 107.7 mAh g^{-1} after 51 cycles. The output voltage of the $LiFePO_4$||TNO cell is 1.8 V due to the low lithiation/delithiation potential of 3.4 V (vs Li/Li^+) for the $LiFePO_4$ cathode.

Layered oxide cathodes possess moderate working potential (2.2−2.5 V) and high specific capacities (about 200 mAh g^{-1}).[99,100] Toshiba Inc. prepared a series of fuel cell batteries with a $TiNb_2O_7$ anode and $LiNi_{0.6}Co_{0.2}Mn_{0.2}O_2$ (NCM) cathode.[18] The fuel cell, with a capacity of 49 Ah, exhibited fast charging, long cycle life, and suitable safety. The batteries reached a SOC of 90% at a charging time of 6 min (10 C) at atmospheric temperature (Figure 10b) and show 80% capacity retention at a low temperature of −10 °C (Figure 10c).

4.1.2. Gassing Issues. Similar to the off-gassing phenomenon of $Li_4Ti_5O_{12}$,[10] TNO fuel cells also suffer from swelling due to a working potential above 1 V and the lack of solid electrolyte interface (SEI) film protection.[29,30] Buannic et al.[29] investigated the gassing behavior of $TiNb_2O_7$ fuel batteries with different specific surface areas of $TiNb_2O_7$ active materials and different cathodes ($LiMn_{1.5}Ni_{0.5}O_4$ and $LiNi_{1/3}Mn_{1/3}Co_{1/3}O_2$). They also tested $Li_4Ti_5O_{12}$ fuel batteries under the same conditions for comparison. It was found that swelling occurred for both $TiNb_2O_7$- and $Li_4Ti_5O_{12}$-based systems, but it was more obvious for the $TiNb_2O_7$ system, likely due to gas evolution from both Ti and Nb cations. The surface area of $TiNb_2O_7$ and the corresponding cathode materials also affect the gassing behavior. The larger the specific surface area of $TiNb_2O_7$, the more gas produced, and due to the electrochemical instability of the $LiMn_{1.5}Ni_{0.5}O_4$ cathode, the swelling behavior of the $TiNb_2O_7$//$LiMn_{1.5}Ni_{0.5}O_4$ system is more obvious than that of the $TiNb_2O_7$//$LiNi_{1/3}Mn_{1/3}Co_{1/3}O_2$ battery.

Although many strategies have been proposed to reduce the gassing in $Li_4Ti_5O_{12}$ fuel batteries, such as surface coating, Al_3F doping, using a PC electrolyte, and introducing an SEI film-forming additive in the electrolyte, little data has been reported for TNO cells.[10] Wu et al.[30] studied the use of vinylene carbonate (VC) in the electrolyte of $LiFePO_4$||$TiNb_2O_7$ pouch cells to hinder gas evolution due to the formation of an effective SEI layer (mainly consisting of Li_2CO_3, LiF, $ROCO_2Li$, and ROLi) on the surface of $TiNb_2O_7$ (Figure 11). Further work on the gassing behavior of TNO should be considered for future industrial applications.

4.2. TNO-Based Hybrid LICs. Hybrid LICs integrate the anode of LIBs that utilize redox reactions during the (de)lithiation process and the cathode of supercapacitors that utilize fast ion absorption and desorption on the surface of the electrode. Theoretically, the device can overcome the limitations of LIBs and supercapacitors.[96]

There are two main challenges for LICs: unbalanced kinetics between the cathode and anode and a mismatch in specific capacities between the cathode and anode (activated carbon (AC) cathodes have a low capacity of ∼40 mAh g^{-1} that decreases with increasing current density). In order to address these issues, research should focus on searching for alternative carbonaceous cathode materials with high electrical conductivity and large specific surface areas to achieve higher specific energy densities. Improvements regarding TNO-based anodes were previously discussed. Figure 12 summarizes the energy densities and power densities of representative TNO-based LIC systems.[19,31,88,101−104] It should be noted that the energy densities and power densities reported in the literatures are based on the masses of active materials, which are between the values of LIBs and supercapacitors.[105,106]

5. SUMMARY AND FUTURE PERSPECTIVES

To meet the demands of large-scale energy storage systems, such as in smart grids and EVs, LIBs must achieve high safety, high energy and power densities, and long lifetimes. TNO anodes have drawn considerable research attention owing to their high reversible capacities, cycling stability, safety, and rate performance. The current work has given an overview of the structure and lithiation mechanisms of TNO materials. Recent advances in the *in situ* characterization methods provide direct experimental evidence regarding the charge storage mechanisms in TNO materials. During lithiation, Li^+ is first intercalated into the lattice along the *b* axis, then it occupies spaces between lattice planes perpendicular to the *b* axis after the insertion amount of lithium reaches about 0.5 Li^+ per transition metal, which makes the lattice volume larger.[22,23] Both the

https://dx.doi.org/10.1021/acs.energyfuels.0c02732
Energy Fuels 2020, 34, 13321−13334

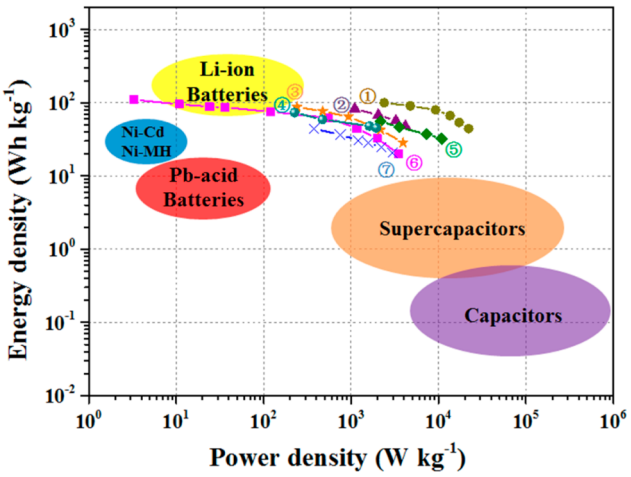

Figure 12. Ragone plots of the TNO-based LICs systems with commercial energy storage devices. Data from the LICs, LIBs, supercapacitors, and capacitors are calculated based on the total mass of active materials: (1) $TiNb_2O_7$@MS/C||AC,[88] (2) $TiNb_2O_7$-750−7 h||AC,[101] (3) $TiNb_2O_7$/HG||AC,[102] (4) $TiNb_2O_7$||graphene,[103] (5) HG-$TiNb_{24}O_{62}$||CN,[19] (6) $TiNb_2O_7$@C||CFs,[104] (7) $TiNb_2O_7$ fibers||AC.[31]

incorporation of defects in TNO and the coating of the rigid conductive layer on the surface of TNO are good solutions to suppress the volume expansion and improve the cycle stability.

Additionally, although TNO has advantages as an anode for LIBs, the electronic conductivity of bulk TNO cannot support fast electron/ion transfer and meet requirements for high-rate applications. Some strategies, such as structure design, elemental doping, size reduction, and composite design, are effective to improve the rate performance of the TNO anode. Combining multiple modification strategies can usually obtain better electrochemical performance than just using a single modification strategy. It should be noted that for preparing TNO nanomaterials and nanocomposites, wet chemical synthesis methods (such as sol−gel,[107] hydrothermal,[108] solvothermal,[24] etc.) are commonly exploited, which is economically unattractive as these require expensive organic reagents as reactants. From a commercial viewpoint, some clean and easily controllable routes to producing high-quality TNO materials at low cost should be developed. Due to their excellent rate performance, TNO electrodes are suitable for both LIBs and LICs fuel-cell systems. Gassing issue problems will be solved for future industrial applications.

TNO anode materials have been extended to sodium ion batteries (SIBs). Huang et al.[109] demonstrated that $TiNb_2O_7$ exhibited capacitive behavior rather than insertion characteristics as an anode material for SIB. They proposed that reducing particle size and increasing specific surface area can improve the capacity of TNO as an anode material for SIB. Shang et al.[79] showed that, compared with pristine $TiNb_2O_7$, $TiNb_2O_7$/CNTs composites possessed enhanced sodium-ion extraction/insertion. The design of the TNO for SIBs will likely involve nanosized material that provides more active surface area for capacitive sodium-ion storage combined with highly conductive frameworks that enhance the collection and the transfer of electrons.

AUTHOR INFORMATION

Corresponding Authors

Meilin Liu − *School of Materials Science and Engineering, Georgia Institute of Technology, Atlanta, Georgia 30332-0245, United States;* orcid.org/0000-0002-6188-2372; Email: meilin.liu@mse.gatech.edu

Shiyou Zheng − *School of Materials Science and Engineering, University of Shanghai for Science and Technology, Shanghai 200093, China;* orcid.org/0000-0002-6614-9567; Email: syzheng@usst.edu.cn

Authors

Tao Yuan − *School of Materials Science and Engineering, University of Shanghai for Science and Technology, Shanghai 200093, China; School of Materials Science and Engineering, Georgia Institute of Technology, Atlanta, Georgia 30332-0245, United States;* orcid.org/0000-0003-3012-1324

Luke Soule − *School of Materials Science and Engineering, Georgia Institute of Technology, Atlanta, Georgia 30332-0245, United States*

Bote Zhao − *School of Materials Science and Engineering, Georgia Institute of Technology, Atlanta, Georgia 30332-0245, United States;* orcid.org/0000-0003-1236-6862

Jie Zou − *School of Materials Science and Engineering, Georgia Institute of Technology, Atlanta, Georgia 30332-0245, United States*

Junhe Yang − *School of Materials Science and Engineering, University of Shanghai for Science and Technology, Shanghai 200093, China*

Complete contact information is available at: https://pubs.acs.org/10.1021/acs.energyfuels.0c02732

Notes

The authors declare no competing financial interest.

ACKNOWLEDGMENTS

We gratefully acknowledge the support of the National Science Foundation of China (51971146, 51671135, 61701267). We also acknowledge the support of the Program of Shanghai Subject Chief Scientist (17XD1403000), Shanghai Outstanding Academic Leaders Plan, the Innovation Program of Shanghai Municipal Education Commission (2019-01-07-00-07-E00015), CBMM, and the U.S. National Science Foundation under award number DMR-1742828.

REFERENCES

(1) Larcher, D.; Tarascon, J. M. Towards greener and more sustainable batteries for electrical energy storage. *Nat. Chem.* **2015**, *7*, 19−29.

(2) Chu, S.; Majumdar, A. Opportunities and challenges for a sustainable energy future. *Nature* **2012**, *488*, 294−303.

(3) Liu, Y.; Zhu, Y.; Cui, Y. Challenges and opportunities towards fast-charging battery materials. *Nat. Energy* **2019**, *4*, 540−550.

(4) Zeng, X.; Li, M.; Abd El-Hady, D.; Alshitari, W.; Al-Bogami, A. S.; Lu, J.; Amine, K. Commercialization of lithium battery technologies for electric vehicles. *Adv. Energy Mater.* **2019**, *9*, 1900161.

(5) Lee, G. H.; Wu, J.; Kim, D.; Cho, K.; Cho, M.; Yang, W.; Kang, Y. M. Reversible anionic redox activities in conventional Li-$Ni_{1/3}Co_{1/3}Mn_{1/3}O_2$ cathodes. *Angew. Chem., Int. Ed.* **2020**, *59*, 8681−8688.

(6) Zhang, P.; Yuan, T.; Pang, Y.; Peng, C.; Yang, J.; Ma, Z.-F.; Zheng, S. Influence of current density on graphite anode failure in lithium-ion batteries. *J. Electrochem. Soc.* **2019**, *166*, A5489−A5495.

(7) Zhao, M.; Zhang, B.; Huang, G.; Dai, W.; Wang, F.; Song, X. Electrochemical performance of modified $LiMn_2O_4$ used as cathode material for an aqueous rechargeable lithium battery. *Energy Fuels* **2012**, *26*, 1214−1219.
(8) Mao, C.; Ruther, R. E.; Li, J.; Du, Z.; Belharouak, I. Identifying the limiting electrode in lithium ion batteries for extreme fast charging. *Electrochem. Commun.* **2018**, *97*, 37−41.
(9) Zhao, B.; Ran, R.; Liu, M.; Shao, Z. A comprehensive review of $Li_4Ti_5O_{12}$-based electrodes for lithium-ion batteries: The latest advancements and future perspectives. *Mater. Sci. Eng., R* **2015**, *98*, 1−71.
(10) Yuan, T.; Tan, Z.; Ma, C.; Yang, J.; Ma, Z.-F.; Zheng, S. Challenges of spinel $Li_4Ti_5O_{12}$ for lithium-ion battery industrial applications. *Adv. Energy Mater.* **2017**, *7*, 1601625.
(11) Luo, S.; Zhang, P.; Yuan, T.; Ruan, J.; Peng, C.; Pang, Y.; Sun, H.; Yang, J.; Zheng, S. Molecular self-assembly of a nanorod N-$Li_4Ti_5O_{12}$/TiO_2/C anode for superior lithium ion storage. *J. Mater. Chem. A* **2018**, *6*, 15755−15761.
(12) Chen, D.; Wang, J. H.; Chou, T. F.; Zhao, B.; El-Sayed, M. A.; Liu, M. Unraveling the nature of anomalously fast energy storage in T-Nb_2O_5. *J. Am. Chem. Soc.* **2017**, *139*, 7071−7081.
(13) Deng, Q.; Fu, Y.; Zhu, C.; Yu, Y. Niobium-based oxides toward advanced electrochemical energy storage: recent advances and challenges. *Small* **2019**, *15*, 1804884.
(14) Koçer, C. P.; Griffith, K. J.; Grey, C. P.; Morris, A. J. First-principles study of localized and delocalized electronic states in crystallographic shear phases of niobium oxide. *Phys. Rev. B: Condens. Matter Mater. Phys.* **2019**, *99*, 075151.
(15) Qu, X.; Liu, Y.; Li, B.; Xing, B.; Huang, G.; Zhang, C.; Hong, S. W.; Yu, J.; Cao, Y. Synthesis of high reversibility anode composite materials using T-Nb_2O_5 and coal-based graphite for lithium-ion battery applications. *Energy Fuels* **2020**, *34*, 3887−3894.
(16) Griffith, K. J.; Forse, A. C.; Griffin, J. M.; Grey, C. P. High-rate intercalation without nanostructuring in metastable Nb_2O_5 bronze phases. *J. Am. Chem. Soc.* **2016**, *138*, 8888−8899.
(17) Yu, H.; Cheng, X.; Zhu, H.; Zheng, R.; Liu, T.; Zhang, J.; Shui, M.; Xie, Y.; Shu, J. Deep insights into kinetics and structural evolution of nitrogen-doped carbon coated $TiNb_{24}O_{62}$ nanowires as high-performance lithium container. *Nano Energy* **2018**, *54*, 227−237.
(18) Takami, N.; Ise, K.; Harada, Y.; Iwasaki, T.; Kishi, T.; Hoshina, K. High-energy, fast-charging, long-life lithium-ion batteries using $TiNb_2O_7$ anodes for automotive applications. *J. Power Sources* **2018**, *396*, 429−436.
(19) Caglar, Y.; Caglar, M.; Ilican, S. XRD, SEM, XPS studies of Sb doped ZnO films and electrical properties of its based Schottky diodes. *Optik* **2018**, *164*, 424−432.
(20) Lou, S.; Cheng, X.; Gao, J.; Li, Q.; Wang, L.; Cao, Y.; Ma, Y.; Zuo, P.; Gao, Y.; Du, C.; Huo, H.; Yin, G. Pseudocapacitive Li^+ intercalation in porous $Ti_2Nb_{10}O_{29}$ nanospheres enables ultra-fast lithium storage. *Energy Storage Mater.* **2018**, *11*, 57−66.
(21) Griffith, K. J.; Seymour, I. D.; Hope, M. A.; Butala, M. M.; Lamontagne, L. K.; Preefer, M. B.; Kocer, C. P.; Henkelman, G.; Morris, A. J.; Cliffe, M. J.; Dutton, S. E.; Grey, C. P. Ionic and electronic conduction in $TiNb_2O_7$. *J. Am. Chem. Soc.* **2019**, *141*, 16706−16725.
(22) Deng, S.; Zhu, H.; Wang, G.; Luo, M.; Shen, S.; Ai, C.; Yang, L.; Lin, S.; Zhang, Q.; Gu, L.; Liu, B.; Zhang, Y.; Liu, Q.; Pan, G.; Xiong, Q.; Wang, X.; Xia, X.; Tu, J. Boosting fast energy storage by synergistic engineering of carbon and deficiency. *Nat. Commun.* **2020**, *11*, 132.
(23) Yu, H.; Lan, H.; Yan, L.; Qian, S.; Cheng, X.; Zhu, H.; Long, N.; Shui, M.; Shu, J. $TiNb_2O_7$ hollow nanofiber anode with superior electrochemical performance in rechargeable lithium ion batteries. *Nano Energy* **2017**, *38*, 109−117.
(24) Deng, S.; Zhang, Y.; Xie, D.; Yang, L.; Wang, G.; Zheng, X.; Zhu, J.; Wang, X.; Yu, Y.; Pan, G.; Xia, X.; Tu, J. Oxygen vacancy modulated $Ti_2Nb_{10}O_{29-x}$ embedded onto porous bacterial cellulose carbon for highly efficient lithium ion storage. *Nano Energy* **2019**, *58*, 355−364.
(25) Yang, C.; Yu, S.; Ma, Y.; Lin, C.; Xu, Z.; Zhao, H.; Wu, S.; Zheng, P.; Zhu, Z.-Z.; Li, J.; Wang, N. Cr^{3+} and Nb^{5+} co-doped $Ti_2Nb_{10}O_{29}$ materials for high-performance lithium-ion storage. *J. Power Sources* **2017**, *360*, 470−479.
(26) Liu, M.; Dong, H.; Zhang, S.; Chen, X.; Sun, Y.; Gao, S.; Xu, J.; Wu, X.; Yuan, A.; Lu, W. Three-dimensional porous $TiNb_2O_7$/CNT-KB composite microspheres as lithium-ion battery anode material. *ChemElectroChem* **2019**, *6*, 3959−3965.
(27) Xiong, J.; Liu, K.; Fei, A.; Yu, L.; Jiang, G.; Yuan, S. Preparation and characterization of Ag/$Ti_2Nb_{10}O_{29}$ composite microspheres anode materials for lithium-ion batteries. *Nano* **2020**, *15*, 2050061.
(28) Han, J.-T.; Huang, Y.-H.; Goodenough, J. B. New anode framework for rechargeable lithium batteries. *Chem. Mater.* **2011**, *23*, 2027−2029.
(29) Buannic, L.; Colin, J.-F.; Chapuis, M.; Chakir, M.; Patoux, S. Electrochemical performances and gassing behavior of high surface area titanium niobium oxides. *J. Mater. Chem. A* **2016**, *4*, 11531−11541.
(30) Wu, X.; Lou, S.; Cheng, X.; Lin, C.; Gao, J.; Ma, Y.; Zuo, P.; Du, C.; Gao, Y.; Yin, G. Unravelling the interface layer formation and gas evolution/suppression on a $TiNb_2O_7$ anode for lithium-ion batteries. *ACS Appl. Mater. Interfaces* **2018**, *10*, 27056−27062.
(31) Aravindan, V.; Sundaramurthy, J.; Jain, A.; Kumar, P. S.; Ling, W. C.; Ramakrishna, S.; Srinivasan, M. P.; Madhavi, S. Unveiling $TiNb_2O_7$ as an insertion anode for lithium ion capacitors with high energy and power density. *ChemSusChem* **2014**, *7*, 1858−63.
(32) Han, J.-T.; Goodenough, J. B. 3-V fuel cell performance of anode framework $TiNb_2O_7$/spinel $LiNi_{0.5}Mn_{1.5}O_4$. *Chem. Mater.* **2011**, *23*, 3404−3407.
(33) Eror, N. G. Self-compensation in niobium-doped TiO_2. *J. Solid State Chem.* **1981**, *38*, 281−287.
(34) Roth, R. S. Thermal stability of long range order in oxides. *Prog. Solid State Chem.* **1980**, *13*, 159−192.
(35) Griffith, K. J.; Senyshyn, A.; Grey, C. P. Structural stability from crystallographic shear in TiO_2-Nb_2O_5 phases: cation ordering and lithiation behavior of $TiNb_{24}O_{62}$. *Inorg. Chem.* **2017**, *56*, 4002−4010.
(36) Lin, C.; Deng, S.; Kautz, D. J.; Xu, Z.; Liu, T.; Li, J.; Wang, N.; Lin, F. Intercalating $Ti_2Nb_{14}O_{39}$ anode materials for fast-charging, high-capacity and safe lithium-ion batteries. *Small* **2017**, *13*, 1702903.
(37) Lee, Y. S.; Ryu, K. S. Study of the lithium diffusion properties and high rate performance of $TiNb_6O_{17}$ as an anode in lithium secondary battery. *Sci. Rep.* **2017**, *7*, 16617.
(38) Yuan, Y.; Yu, H.; Cheng, X.; Zheng, R.; Liu, T.; Peng, N.; Long, N.; Shui, M.; Shu, J. Preparation of $TiNb_6O_{17}$ nanospheres as high-performance anode candidates for lithium-ion storage. *Chem. Eng. J.* **2019**, *374*, 937−946.
(39) Yamaguchi, O.; Tomihisa, D.; Ogiso, N.; Shimizu, K. Crystallization of Monoclinic $2TiO_2{\cdot}5Nb_2O_5$. *J. Am. Ceram. Soc.* **1986**, *69*, C-150−C-151.
(40) Hu, L.; Luo, L.; Tang, L.; Lin, C.; Li, R.; Chen, Y. $Ti_2Nb_{2x}O_{4+5x}$ anode materials for lithium-ion batteries: a comprehensive review. *J. Mater. Chem. A* **2018**, *6*, 9799−9815.
(41) Roth, R. S.; Wadsley, A. D. Mixed oxides of titanium and niobium: the crystal structure of $TiNb_{24}O_{62}(TiO_2{\cdot}12Nb_2O_5)$. *Acta Crystallogr.* **1965**, *18*, 724−730.
(42) Gasperin, M. Affinement de la structure de $TiNb_2O_7$ et répartition des cations. *J. Solid State Chem.* **1984**, *53*, 144−147.
(43) Wadsley, A. D. Mixed oxides of titanium and niobium. II. The crystal structures of the dimorphic forms $Ti_2Nb_{10}O_{29}$. *Acta Crystallogr.* **1961**, *14*, 664−670.
(44) Wu, X.; Miao, J.; Han, W.; Hu, Y.-S.; Chen, D.; Lee, J.-S.; Kim, J.; Chen, L. Investigation on $Ti_2Nb_{10}O_{29}$ anode material for lithium-ion batteries. *Electrochem. Commun.* **2012**, *25*, 39−42.
(45) Dylla, A. G.; Henkelman, G.; Stevenson, K. J. Lithium insertion in nanostructured TiO(2)(B) architectures. *Acc. Chem. Res.* **2013**, *46*, 1104−1112.
(46) Lübke, M.; Shin, J.; Marchand, P.; Brett, D.; Shearing, P.; Liu, Z.; Darr, J. A. Highly pseudocapacitive Nb-doped TiO_2 high power anodes for lithium-ion batteries. *J. Mater. Chem. A* **2015**, *3*, 22908−22914.
(47) Wang, Y.; Smarsly, B. M.; Djerdj, I. Niobium doped TiO_2 with mesoporosity and its application for lithium insertion. *Chem. Mater.* **2010**, *22*, 6624−6631.

(48) Zhai, X.; Liu, J.; Zhao, Y.; Chen, C.; Zhao, X.; Li, J.; Jin, H. Oxygen vacancy boosted the electrochemistry performance of Ti^{4+} doped Nb_2O_5 toward lithium ion battery. *Appl. Surf. Sci.* **2020**, *499*, 143905.

(49) Wagemaker, M.; Borghols, W. J. H.; Mulder, F. M. Large impact of particle size on insertion reactions. A case for anatase Li_xTiO_2. *J. Am. Chem. Soc.* **2007**, *129*, 4323−4327.

(50) Li, H.; Shen, L.; Pang, G.; Fang, S.; Luo, H.; Yang, K.; Zhang, X. $TiNb_2O_7$ nanoparticles assembled into hierarchical microspheres as high-rate capability and long-cycle-life anode materials for lithium ion batteries. *Nanoscale* **2015**, *7*, 619−24.

(51) Deng, S.; Chao, D.; Zhong, Y.; Zeng, Y.; Yao, Z.; Zhan, J.; Wang, Y.; Wang, X.; Lu, X.; Xia, X.; Tu, J. Vertical graphene/$Ti_2Nb_{10}O_{29}$/hydrogen molybdenum bronze composite arrays for enhanced lithium ion storage. *Energy Storage Mater.* **2018**, *12*, 137−144.

(52) Dai, H.; Yang, C.; Ou, X.; Liang, X.; Xue, H.; Wang, W.; Xu, G. Unravelling the electrochemical properties and thermal behavior of $NaNi_{2/3}Sb_{1/3}O_2$ cathode for sodium-ion batteries by in situ X-ray diffraction investigation. *Electrochim. Acta* **2017**, *257*, 146−154.

(53) Guo, B.; Yu, X.; Sun, X.-G.; Chi, M.; Qiao, Z.-A.; Liu, J.; Hu, Y.-S.; Yang, X.-Q.; Goodenough, J. B.; Dai, S. A long-life lithium-ion battery with a highly porous $TiNb_2O_7$ anode for large-scale electrical energy storage. *Energy Environ. Sci.* **2014**, *7*, 2220−2226.

(54) Gao, J.; Cheng, X.; Lou, S.; Ma, Y.; Zuo, P.; Du, C.; Gao, Y.; Yin, G. Self-doping $Ti_{1-x}Nb_{2+x}O_7$ anode material for lithium-ion battery and its electrochemical performance. *J. Alloys Compd.* **2017**, *728*, 534−540.

(55) Cheng, Q.; Liang, J.; Zhu, Y.; Si, L.; Guo, C.; Qian, Y. Bulk $Ti_2Nb_{10}O_{29}$ as long-life and high-power Li-ion battery anodes. *J. Mater. Chem. A* **2014**, *2*, 17258−17262.

(56) Catti, M.; Pinus, I.; Knight, K. Lithium insertion properties of $LiTiNb_2O_7$ investigated by neutron diffraction and first-principles modelling. *J. Solid State Chem.* **2015**, *229*, 19−25.

(57) Lu, X.; Jian, Z.; Fang, Z.; Gu, L.; Hu, Y.-S.; Chen, W.; Wang, Z.; Chen, L. Atomic-scale investigation on lithium storage mechanism in $TiNb_2O_7$. *Energy Environ. Sci.* **2011**, *4*, 2638.

(58) Wang, W. L.; Oh, B.-Y.; Park, J.-Y.; Ki, H.; Jang, J.; Lee, G.-Y.; Gu, H.-B.; Ham, M.-H. Solid-state synthesis of $Ti_2Nb_{10}O_{29}$/reduced graphene oxide composites with enhanced lithium storage capability. *J. Power Sources* **2015**, *300*, 272−278.

(59) Babu, B.; Shaijumon, M. M. Studies on kinetics and diffusion characteristics of lithium ions in $TiNb_2O_7$. *Electrochim. Acta* **2020**, *345*, 136208.

(60) Voskanyan, A. A.; Abramchuk, M.; Navrotsky, A. Entropy Stabilization of TiO_2-Nb_2O_5 Wadsley-Roth Shear Phases and Their Prospects for Lithium-Ion Battery Anode Materials. *Chem. Mater.* **2020**, *32*, 5301−5308.

(61) Sheppard, L. R.; Bak, T.; Nowotny, J. Electrical properties of niobium-doped titanium dioxide. 1. Defect disorder. *J. Phys. Chem. B* **2006**, *110*, 22447−22454.

(62) Yan, W.; Liu, X. Niobium-doped TiO_2: effect of an interstitial oxygen atom on the charge state of niobium. *Inorg. Chem.* **2019**, *58*, 3090−3098.

(63) Inada, R.; Mori, T.; Kumasaka, R.; Ito, R.; Tojo, T.; Sakurai, Y. Characterization of vacuum-annealed $TiNb_2O_7$ as high potential anode material for lithium-ion battery. *Int. J. Appl. Ceram. Technol.* **2019**, *16*, 264−272.

(64) Takashima, T.; Tojo, T.; Inada, R.; Sakurai, Y. Characterization of mixed titanium-niobium oxide $Ti_2Nb_{10}O_{29}$ annealed in vacuum as anode material for lithium-ion battery. *J. Power Sources* **2015**, *276*, 113−119.

(65) Zhang, Y.; Zhang, M.; Liu, Y.; Zhu, H.; Wang, L.; Liu, Y.; Xue, M.; Li, B.; Tao, X. Oxygen vacancy regulated $TiNb_2O_7$ compound with enhanced electrochemical performance used as anode material in Li-ion batteries. *Electrochim. Acta* **2020**, *330*, 135299.

(66) Yao, Z.; Xia, X.; Zhang, S.; Zhou, C.-a.; Pan, G.; Xiong, Q.; Wang, Y.; Wang, X.; Tu, J. Oxygen defect boosted N-doped $Ti_2Nb_{10}O_{29}$ anchored on core-branch carbon skeleton for both high-rate liquid & solid-state lithium ion batteries. *Energy Storage Mater.* **2020**, *25*, 555−562.

(67) Yang, C.; Lin, C.; Lin, S.; Chen, Y.; Li, J. $Cu_{0.02}Ti_{0.94}Nb_{2.04}O_7$: An advanced anode material for lithium-ion batteries of electric vehicles. *J. Power Sources* **2016**, *328*, 336−344.

(68) Hu, L.; Lu, R.; Tang, L.; Xia, R.; Lin, C.; Luo, Z.; Chen, Y.; Li, J. $TiCr_{0.5}Nb_{10.5}O_{29}$/CNTs nanocomposite as an advanced anode material for high-performance Li^+-ion storage. *J. Alloys Compd.* **2018**, *732*, 116−123.

(69) Deng, S.; Zhu, H.; Liu, B.; Yang, L.; Wang, X.; Shen, S.; Zhang, Y.; Wang, J.; Ai, C.; Ren, Y.; Liu, Q.; Lin, S.; Lu, Y.; Pan, G.; Wu, J.; Xia, X.; Tu, J. Synergy of ion doping and spiral array architecture on $Ti_2Nb_{10}O_{29}$: a new way to achieve high-power electrodes. *Adv. Funct. Mater.* **2020**, *30*, 2002665.

(70) Lin, C.; Yu, S.; Wu, S.; Lin, S.; Zhu, Z.-Z.; Li, J.; Lu, L. $Ru_{0.01}Ti_{0.99}Nb_2O_7$ as an intercalation-type anode material with a large capacity and high rate performance for lithium-ion batteries. *J. Mater. Chem. A* **2015**, *3*, 8627−8635.

(71) Wen, X.; Ma, C.; Du, C.; Liu, J.; Zhang, X.; Qu, D.; Tang, Z. Enhanced electrochemical properties of vanadium-doped titanium niobate as a new anode material for lithium-ion batteries. *Electrochim. Acta* **2015**, *186*, 58−63.

(72) Song, H.; Kim, Y. T. A Mo-doped $TiNb_2O_7$ anode for lithium-ion batteries with high rate capability due to charge redistribution. *Chem. Commun.* **2015**, *51*, 9849−52.

(73) Song, K.; Seo, D.-H.; Jo, M. R.; Kim, Y.-I.; Kang, K.; Kang, Y.-M. Tailored Oxygen Framework of $Li_4Ti_5O_{12}$ Nanorods for High-Power Li Ion Battery. *J. Phys. Chem. Lett.* **2014**, *5*, 1368−1373.

(74) Tang, Y.; Deng, S.; Shi, S.; Wu, L.; Wang, G.; Pan, G.; Lin, S.; Xia, X. Ultrafast and durable lithium ion storage enabled by intertwined carbon nanofiber/$Ti_2Nb_{10}O_{29}$ core-shell arrays. *Electrochim. Acta* **2020**, *332*, 135433.

(75) Wang, G.; Wen, Z.; Du, L.; Yang, Y.-E.; Li, S.; Sun, J.; Ji, S. Hierarchical Ti-Nb oxide microspheres with synergic multiphase structure as ultra-long-life anode materials for lithium-ion batteries. *J. Power Sources* **2017**, *367*, 106−115.

(76) Luo, J.; Peng, J.; Zeng, P.; Xiao, W.; Li, W.; Wu, Z.; Wang, Y.; Miao, C.; Chen, G.; Shu, H.; Wang, X. Controlled fabrication and performances of single-core/dual-shell hierarchical structure m-TNO@TiC@NC anode composite for lithium-ion batteries. *Electrochim. Acta* **2020**, *341*, 136072.

(77) Yin, L.; Pham-Cong, D.; Jeon, I.; Kim, J.-P.; Cho, J.; Jeong, S.-Y.; Woo Lee, H.; Cho, C.-R. Electrochemical performance of vertically grown WS_2 layers on $TiNb_2O_7$ nanostructures for lithium-ion battery anodes. *Chem. Eng. J.* **2020**, *382*, 122800.

(78) Kim, H.; Lee, Y.; Byun, D.; Choi, W. $TiNb_2O_7$ microsphere anchored by polydopamine-modified graphene oxide as a superior anode material in lithium-ion batteries. *Int. J. Energy Res.* **2020**, *44*, 4986−4996.

(79) Shang, B.; Peng, Q.; Jiao, X.; Xi, G.; Hu, X. $TiNb_2O_7$/carbon nanotube composites as long cycle life anode for sodium-ion batteries. *Ionics* **2019**, *25*, 1679−1688.

(80) Luo, J.; Peng, J.; Zeng, P.; Wu, Z.; Li, J.; Li, W.; Huang, Y.; Chang, B.; Wang, X. $TiNb_2O_7$ nano-particle decorated carbon cloth as flexible self-support anode material in lithium-ion batteries. *Electrochim. Acta* **2020**, *332*, 135469.

(81) Wan, G.; Yang, L.; Shi, S.; Tang, Y.; Xu, X.; Wang, G. $Ti_2Nb_{10}O_{29}$ microspheres coated with ultrathin N-doped carbon layers by atomic layer deposition for enhanced lithium storage. *Chem. Commun.* **2019**, *55*, 517−520.

(82) Lyu, H.; Li, J.; Wang, T.; Thapaliya, B. P.; Men, S.; Jafta, C. J.; Tao, R.; Sun, X.-G.; Dai, S. Carbon coated porous titanium niobium oxides as anode materials of lithium-ion batteries for extreme fast charge applications. *ACS Appl. Energy Mater.* **2020**, *3*, 5657−5665.

(83) Yang, Y.; Yue, Y.; Wang, L.; Cheng, X.; Hu, Y.; Yang, Z.-z.; Zhang, R.; Jin, B.; Sun, R. Facile synthesis of mesoporous $TiNb_2O_7$/C microspheres as long-life and high-power anodes for lithium-ion batteries. *Int. J. Hydrogen Energy* **2020**, *45*, 12583−12592.

(84) Yao, Z.; Xia, X.; Zhang, Y.; Xie, D.; Ai, C.; Lin, S.; Wang, Y.; Deng, S.; Shen, S.; Wang, X.; Yu, Y.; Tu, J. Superior high-rate lithium-

ion storage on $Ti_2Nb_{10}O_{29}$ arrays via synergistic TiC/C skeleton and N-doped carbon shell. *Nano Energy* **2018**, *54*, 304−312.
(85) Liu, X.; Wang, H.; Zhang, S.; Liu, G.; Xie, H.; Ma, J. Design of well-defined porous $Ti_2Nb_{10}O_{29}$/C microspheres assembled from nanoparticles as anode materials for high-rate lithium ion batteries. *Electrochim. Acta* **2018**, *292*, 759−768.
(86) Sun, R.; Tao, Y.; Sun, H.; Chen, W.; Liu, G.; Yue, Y.; Hu, M.; Liu, M. Simple synthesis of $TiNb_6O_{17}$/C composite toward high-rate lithium storage. *J. Mater. Sci.* **2019**, *54*, 14825−14833.
(87) Mao, W.; Liu, K.; Guo, G.; Liu, G.; Bao, K.; Guo, J.; Hu, M.; Wang, W.; Li, B.; Zhang, K.; Qian, Y. Preparation and Electrochemical Performance of $Ti_2Nb_{10}O_{29}$/Ag Composite as Anode Materials for Lithium Ion Batteries. *Electrochim. Acta* **2017**, *253*, 396−402.
(88) Yao, M.; Liu, A.; Xing, C.; Li, B.; Pan, S.; Zhang, J.; Su, P.; Zhang, H. Asymmetric supercapacitor comprising a core-shell $TiNb_2O_7$@MoS_2/C anode and a high voltage ionogel electrolyte. *Chem. Eng. J.* **2020**, *394*, 124883.
(89) Yuan, T.; Zhao, B.; Cai, R.; Zhou, Y.; Shao, Z. Electrospinning based fabrication and performance improvement of film electrodes for lithium-ion batteries composed of TiO_2 hollow fibers†. *J. Mater. Chem.* **2011**, *21*, 15041−15048.
(90) Krajewski, M.; Michalska, M.; Hamankiewicz, B.; Ziolkowska, D.; Korona, K. P.; Jasinski, J. B.; Kaminska, M.; Lipinska, L.; Czerwinski, A. $Li_4Ti_5O_{12}$ modified with Ag nanoparticles as an advanced anode material in lithium-ion batteries. *J. Power Sources* **2014**, *245*, 764−771.
(91) Zhang, Y.; Zhang, P.; Li, B.; Zhang, S.; Liu, K.; Hou, R.; Zhang, X.; Silva, S. R. P.; Shao, G. Vertically aligned graphene nanosheets on multi-yolk/shell structured TiC@C nanofibers for stable Li-S batteries. *Energy Storage Mater.* **2020**, *27*, 159−168.
(92) Song, S.; Li, W.; Deng, Y.-P.; Ruan, Y.; Zhang, Y.; Qin, X.; Chen, Z. TiC supported amorphous MnOx as highly efficient bifunctional electrocatalyst for corrosion resistant oxygen electrode of Zn-air batteries. *Nano Energy* **2020**, *67*, 104208.
(93) Kim, H.; Kim, M.; Yoon, Y. H.; Nguyen, Q. H.; Kim, I. T.; Hur, J.; Lee, S. G. Sb_2Te_3-TiC-C nanocomposites for the high-performance anode in lithium-ion batteries. *Electrochim. Acta* **2019**, *293*, 8−18.
(94) Yuan, T.; Li, W.-T.; Zhang, W.; He, Y.-S.; Zhang, C.; Liao, X.-Z.; Ma, Z.-F. One-pot spray-dried graphene sheets-encapsulated nano-$Li_4Ti_5O_{12}$ microspheres for a hybrid BatCap system. *Ind. Eng. Chem. Res.* **2014**, *53*, 10849−10857.
(95) Luo, S.; Yuan, T.; Soule, L.; Ruan, J.; Zhao, Y.; Sun, D.; Yang, J.; Liu, M.; Zheng, S. Enhanced ionic/electronic transport in nano-TiO_2/sheared CNT composite electrode for Na^+ insertion-based hybrid ion-capacitors. *Adv. Funct. Mater.* **2020**, *30*, 1908309.
(96) Li, G.; Yang, Z.; Yin, Z.; Guo, H.; Wang, Z.; Yan, G.; Liu, Y.; Li, L.; Wang, J. Non-aqueous dual-carbon lithium-ion capacitors: a review. *J. Mater. Chem. A* **2019**, *7*, 15541−15563.
(97) Ashish, A. G.; Arunkumar, P.; Babu, B.; Manikandan, P.; Sarang, S.; Shaijumon, M. M. $TiNb_2O_7$/graphene hybrid material as high performance anode for lithium-ion batteries. *Electrochim. Acta* **2015**, *176*, 285−292.
(98) Amin, R.; Muralidharan, N.; Petla, R. K.; Ben Yahia, H.; Jassim Al-Hail, S. A.; Essehli, R.; Daniel, C.; Khaleel, M. A.; Belharouak, I. Research advances on cobalt-free cathodes for Li-ion batteries-The high voltage $LiMn_{1.5}N_{i0.5}O_4$ as an example. *J. Power Sources* **2020**, *467*, 228318.
(99) Li, H.; Wang, Y.; He, X.; Li, Q.; Lian, C.; Wang, Z. Effects of structure parameters on the thermal performance of a ternary lithium-ion battery under fast charging conditions. *Energy Fuels* **2020**, *34*, 8891−8904.
(100) Chakraborty, A.; Kunnikuruvan, S.; Kumar, S.; Markovsky, B.; Aurbach, D.; Dixit, M.; Major, D. T. Layered cathode materials for lithium-ion batteries: review of computational studies on $LiNi_{1-x-y}Co_xMn_yO_2$ and $LiNi_{1-x-y}Co_xAl_yO_2$. *Chem. Mater.* **2020**, *32*, 915−952.
(101) Deng, B.; Dong, H.; Lei, T.; Yue, N.; Xiao, L.; Liu, J. Post-annealing tailored 3D cross-linked $TiNb_2O_7$ nanorod electrode: towards superior lithium storage for flexible lithium-ion capacitors. *Sci. China Mater.* **2020**, *63*, 492−504.
(102) Jiao, X.; Hao, Q.; Xia, X.; Yao, D.; Ouyang, Y.; Lei, W. Boosting long-cycle-life energy storage with holey graphene supported $TiNb_2O_7$ network nanostructure for lithium ion hybrid supercapacitors. *J. Power Sources* **2018**, *403*, 66−75.
(103) Li, H. S.; Shen, L. F.; Wang, J.; Fang, S.; Zhang, Y. X.; Dou, H.; Zhang, X. G. Three-dimensionally ordered porous $TiNb_2O_7$ nanotubes: a superior anode material for next generation hybrid supercapacitors. *J. Mater. Chem. A* **2015**, *3*, 16785−16790.
(104) Wang, X.; Shen, G. Intercalation pseudo-capacitive $TiNb_2O_7$@carbon electrode for high-performance lithium ion hybrid electrochemical supercapacitors with ultrahigh energy density. *Nano Energy* **2015**, *15*, 104−115.
(105) Kouchachvili, L.; Yaïci, W.; Entchev, E. Hybrid battery/supercapacitor energy storage system for the electric vehicles. *J. Power Sources* **2018**, *374*, 237−248.
(106) Wang, R.; Yu, J.; Islam, F.; Tahmasebi, A.; Lee, S.; Chen, Y. State-of-the-art research and applications of carbon foam composite materials as electrodes for high-capacity lithium batteries. *Energy Fuels* **2020**, *34*, 7935−7954.
(107) Shim, H.; Lim, E.; Fleischmann, S.; Quade, A.; Tolosa, A.; Presser, V. Nanosized titanium niobium oxide/carbon electrodes for lithium-ion energy storage applications. *Sustainable Energy Fuels* **2019**, *3*, 1776−1789.
(108) Ise, K.; Morimoto, S.; Harada, Y.; Takami, N. Large lithium storage in highly crystalline $TiNb_2O_7$ nanoparticles synthesized by a hydrothermal method as anodes for lithium-ion batteries. *Solid State Ionics* **2018**, *320*, 7−15.
(109) Huang, Y.; Li, X.; Luo, J.; Wang, K.; Zhang, Q.; Qiu, Y.; Sun, S.; Liu, S.; Han, J.; Huang, Y. Enhancing sodium-ion storage behaviors in $TiNb_2O_7$ by mechanical ball milling. *ACS Appl. Mater. Interfaces* **2017**, *9*, 8696−8703.

https://dx.doi.org/10.1021/acs.energyfuels.0c02732
Energy Fuels 2020, 34, 13321−13334